Paleoceanography and Paleoclimatology

RESEARCH ARTICLE
10.1029/2020PA004061

Key Points:

- Bottom water temperature in the Fram Strait increased up to 5°C during Heinrich Stadials (HSs) due to subsurface flow of Atlantic water
- During HSs, a strong halocline prevented heat loss from the Atlantic water, from 45°N in the North Atlantic to the Arctic Ocean >79°N
- Release of subsurface heat from this vast area contributed to the abrupt regional atmospheric warmings at the start of Greenland Interstadials

Supporting Information:

- Supporting Information S1

Correspondence to:
N. El bani Altuna,
naima.e.altuna@uit.no

Citation:
El bani Altuna, N., Ezat, M. M., Greaves, M., & Rasmussen, T. L. (2021). Millennial-scale changes in bottom water temperature and water mass exchange through the Fram Strait 79°N, 63-13 ka. *Paleoceanography and Paleoclimatology*, *36*, e2020PA004061. https://doi.org/10.1029/2020PA004061

Received 19 JUL 2020
Accepted 21 DEC 2020

Millennial-Scale Changes in Bottom Water Temperature and Water Mass Exchange Through the Fram Strait 79°N, 63-13 ka

N. El bani Altuna[1], M. M. Ezat[1,2], M. Greaves[3], and T. L. Rasmussen[1]

[1]Department of Geology, CAGE - Centre for Arctic Gas Hydrate, Environment and Climate, UiT, Arctic University of Norway, Tromsø, Norway, [2]Department of Geology, Faculty of Science, Beni-Suef University, Beni-Suef, Egypt, [3]Department of Earth Sciences, Godwin Laboratory for Palaeoclimate Research, University of Cambridge, Cambridge, UK

Abstract The Svalbard margin, in the eastern Fram Strait with its high sediment accumulation, form a key area for the reconstruction of water mass and heat exchange between the North Atlantic and Arctic Ocean in relation to abrupt climate changes as seen in glacial Greenland Interstadial and Greenland Stadial (GI-GS) events. Here, we present a bottom water temperature (BWT) record from the northern Nordic Seas (79°N) at 1,273 m water depth based on benthic foraminiferal Mg/Ca. The BWT reconstructions, combined with benthic foraminiferal stable isotopes, benthic foraminiferal fauna compositions and ice-rafted debris (IRD), reveal at least two distinctive scenarios for the GI-GS events during the last glacial period (13–63 ka). During GIs, conditions were similar to modern with high productivity, low BWT and deep convection. During GS6, GS8, and GS15 and during Heinrich Stadials (HSs), BWT increased up to 5°C ± 1°C generally concomitant with low planktic and benthic $\delta^{18}O$. Our results suggest, that during some GSs and HSs, deep water generation was reduced, allowing the subsurface Atlantic water (AW) to thicken and deepen down to at least the core site depth. A strong halocline during HSs and GSs prevented heat release from the subsurface AW, which we can now trace from 45°N in the North Atlantic to the Arctic Ocean >79°N. Surfacing of the salty Atlantic subsurface water preconditioned the Nordic seas for convection. Release of the subsurface heat from this vast reservoir must have contributed to the large and abrupt atmospheric warmings at the start of GIs.

Plain Language Summary The Fram Strait is an area where warm and salty Atlantic water (AW) enters the Arctic Ocean from the North Atlantic Ocean. As it flows northwards in the Nordic Seas, the AW mass releases heat to the atmosphere and sinks to form deep cold water, both moderating regional climate and driving deep ocean circulation. To better understand future changes in ocean circulation and interactions under ongoing climate change, it is necessary to study past oceanic changes in relation to climate change. We investigated benthic foraminifera (single-celled organisms with shells living at the sea floor) with the aim of reconstructing bottom water temperature variations during the last ice age during abrupt atmospheric warmings and coolings on millennial time scales. Our results show that during events of extremely low atmospheric temperature, the deep ocean from the northern North Atlantic to the Arctic Ocean was warmer than today. The ocean surface was cold and stratified due to the presence of polar meltwater. The accumulation of subsurface heat in this vast area toward the end of these periods and decrease of meltwater supply probably broke the stratification, and the subsequent heat release from the ocean to the atmosphere contributed to the abrupt atmospheric warming and onset of renewed convection and cold deep water formation.

1. Introduction

During the last glacial period, the climate of the northern hemisphere was affected by abrupt millennial-scale climate changes called Dansgaard-Oeschger (D-O) events (Dansgaard et al., 1982, 1993; Johnsen et al., 1992). Greenland ice cores record ~25 sudden atmospheric warmings in the order of 8°C–16°C from cold stadials (Greenland Stadials, GS) to warm interstadials (Greenland Interstadials, GI) occurring within a few decades (Dansgaard et al., 1993; Huber et al., 2006; Landais et al., 2006; S.O. Rasmussen et al., 2014a). In marine records from the Nordic Seas, GIs are generally short (from centuries to millennia) with variable

hydrographic conditions, whereas GSs are long-lasting (millennia) and characterized by generally more stable and stratified hydrographic conditions (e.g., T. L. Rasmussen & Thomsen, 2004). During some GS events, layers with large amounts of ice-rafted debris (IRD) and dominance of the polar planktic foraminifera *Neogloboquadrina pachyderma* have been found at mid-latitudes in the Northern Hemisphere. These layers were deposited during Heinrich events occurring during Heinrich Stadials (HSs) or Heinrich-like Stadials, depending on the origin of the IRD (e.g., Bond & Lotti, 1995; Elliot et al., 2001; Hemming, 2004). These events are characterized by massive freshwater supply from the melting of icebergs traversing the North Atlantic Ocean (Bond et al., 1993; Heinrich, 1988).

In the Nordic Seas, the development of GI-GS events have been studied combining (sub)surface and bottom water proxy tools (e.g., foraminiferal $\delta^{18}O$ and Mg/Ca, microfossil assemblages, sea-ice proxy IP_{25}) to reconstruct surface and bottom water conditions and sea-ice extent (e.g., Dokken & Hald, 1996; Ezat et al., 2016; Hoff et al., 2016; Jessen & Rasmussen, 2019; Müller & Stein, 2014; T. L. Rasmussen & Thomsen, 2004; T. L. Rasmussen et al., 1996a, 1996b, 2014a; Sadatzki et al., 2019; Sarnthein et al., 2001; Wary et al., 2017). Many previous studies propose scenarios with an active warm Atlantic water (AW) inflow to the Nordic Seas during GIs similar to modern ocean circulation. The inflow contributes to open ocean convection and formation of cold deep water in the Nordic Seas (Ezat et al., 2014; T. L. Rasmussen & Thomsen, 2004; T. L. Rasmussen et al., 1996a, 1996b).

During cold GS and HS events, proxy records from the Nordic Seas and the subpolar North Atlantic show that the Atlantic warm water was subducted beneath a strong halocline, occupying the intermediate depths in the absence of deep water formation under extensive sea-ice cover (e.g., Ezat et al., 2014, 2017, 2019; Hoff et al., 2016; Marcott et al., 2011; T. L. Rasmussen & Thomsen, 2004; T. L. Rasmussen et al., 1996a, 1996b, 2014b). This is in agreement with several modeling studies that simulated D-O-like events in response to freshwater forcing, that caused changes in deep convection and the northward transport of heat (e.g., Brady & Otto-Bliesner, 2011; Ganopolski & Rahmstorf, 2001; Knutti et al., 2004).

Bottom water temperature (BWT) has been investigated in the southern part of the Nordic Seas for the last 60 Kyr using Mg/Ca measured in tests of benthic foraminifera (Ezat et al., 2014). Sessford et al. (2018, 2019) investigated the evolution of BWT for a shorter ca. 8 ka time interval of four D-O events northwest of Iceland and in a nearby record to Ezat et al. (2014). The results show a consistent warming at intermediate depths during GSs, and particularly HSs, with temperatures reaching up to 5.5°C at depths between 1,200 and 1,500 m water depth indicating low or no convection in the Nordic Seas. In the central Arctic Ocean, temperature reconstructions for the intermediate depths (ca. 800–1,500 m water depth) also show millennial-scale changes (Cronin et al., 2012, 2017), but very low sedimentation rates prevented the study of BWT on detailed D-O time scales. The reconstruction of variations in BWT thus constitutes an indirect tool to study the changes in deep-water formation in the past and can be used to trace the circulation of the different water masses and the Atlantic-Arctic Ocean exchange through the Fram Strait.

Here, we present a benthic foraminiferal Mg/Ca record in order to quantify changes in BWT and trace the AW inflow to the Arctic Ocean in relation to millennial-scale climate change. The core site is located in the Fram Strait at 1,273 m water depth on the western Svalbard slope at 79°N. The BWT are compared with benthic foraminiferal assemblage composition, foraminiferal stable isotopes, grain-size distribution and IRD content in order to reconstruct the paleoceanographic development of this high-latitude area.

2. Regional Setting

2.1. Modern Oceanography

The Fram Strait constitutes the major pathway for the exchange of deep and intermediate water masses between the Atlantic and the Arctic Oceans (Aagaard & Coachman, 1968; Hopkins, 1991). In the eastern part of the Fram Strait, the West Spitsbergen Current (WSC) transports warm Atlantic surface water northwards along the western Svalbard slope (Figure 1a). The AW carries heat and salt into the Arctic Ocean and keeps the western Svalbard area free of sea ice today (Hopkins, 1991). In the northern part of the Fram Strait, the AW slightly cools and deepens to become the intermediate Atlantic layer that flows below the thick, cold, low salinity Polar Surface Water in the Arctic Ocean (Aagaard et al., 1981; Rudels, 1987).

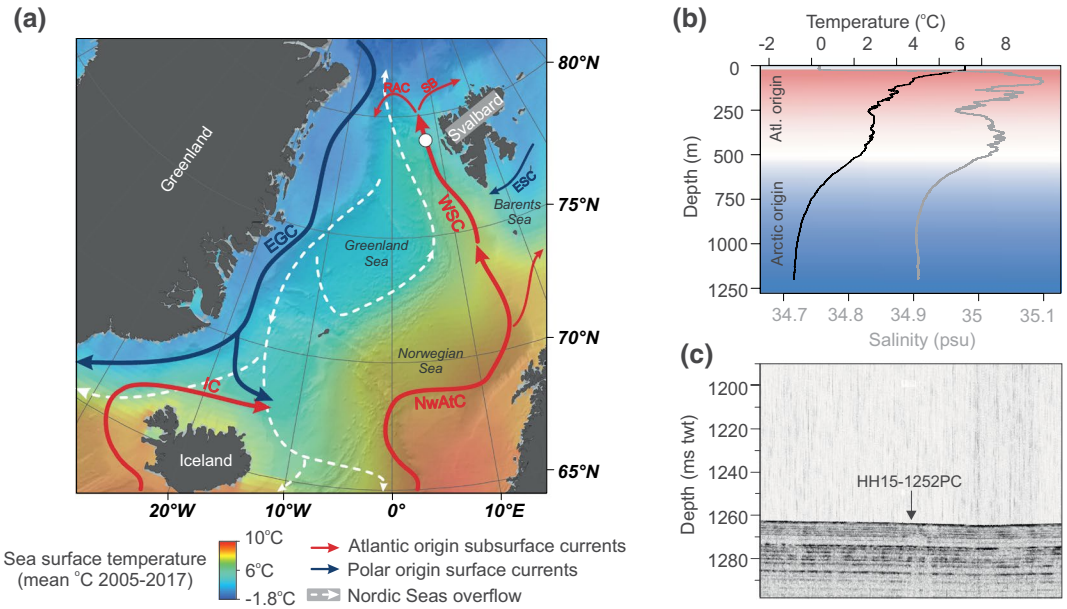

Figure 1. (a) Map of the Greenland Sea showing the position of piston core HH15-1252PC at Vestnesa Ridge (white circle). Main surface and deep currents and mean annual sea surface temperature for the 2005–2017 period (Locarnini et al., 2018) are also shown. The location of other cores from the literature used in the discussion are shown in Figure S1. (b) CTD (Conductivity-Temperature-Depth) data and (c) chirp image taken during core retrieval showing undisturbed, stratified sediments. Abbreviations: EGC, East Greenland Current; ESC, East Spitsbergen Current; IC, Irminger Current; NwAtC, Norwegian Atlantic Current; RAC, Return Atlantic Current; SB, Svalbard Branch; WSC, West Spitsbergen Current.

In the western part of the Fram Strait, the East Greenland Current (EGC) flows southwards along East Greenland and into the Atlantic Ocean (Figure 1a). The EGC carries cold and low saline polar surface water from the Transpolar Drift in the Arctic Ocean overlaying the warmer and saltier Return Atlantic Water (RAW), a branch of the WSC that diverges southward over the Yermak Plateau as an intermediate depth layer of AW. The Arctic Ocean Deep Water is found below RAW (Hopkins, 1991). The mixing and sinking of cold and saline surface waters in the Nordic Seas generate overflows across the Greenland-Scotland Ridge, which contributes to the formation of North Atlantic Deep Water (NADW).

A conductivity-temperature-depth taken close to the core location north of Vestnesa Ridge at the northwestern Svalbard margin in July 2015 shows that the water column here is characterized by a thin mixed surface water layer ($T = 7$°C, $S = 34.8$) generated by the mixing of meltwater and AW (Figure 1b). The main core of AW ($T = 1$°C–4°C, $S = 34.9$–35) occurs beneath the mixed surface layer in the upper 500–800 m of the water column. The bottom water at the core site is influenced by Greenland Sea Intermediate Water (GSIW), with an average temperature of −0.8°C (Figure 1b). No seasonal changes in BWT in the area for the 1981–2010 period were recorded (Locarnini et al., 2018).

2.2. Geological Settings

The sediments along the western Svalbard margin date mainly from the Late Pliocene to Quaternary (Eidvin et al., 1993; Vorren et al., 1998). Vestnesa Ridge is a sediment drift located at 79°N in the eastern part of the Fram Strait (Eiken & Hinz, 1993; Howe et al., 2007) (Figure 1a). The shallow sedimentary evolution of this area is closely related to the strength of the bottom water contour currents and the ridge is flanked by thick contourite deposits (Eiken & Hinz, 1993; Howe et al., 2007; Ottesen et al., 2005). Methane release from the seafloor occurs from a series of pockmarks at the crest of Vestnesa Ridge (e.g., Bunz et al., 2012; Vogt et al., 1994). Bünz et al. (2012) reported at least six active venting pockmarks at 1,200 m water depth in the eastern part of Vestnesa Ridge.

Table 1
Radiocarbon Dates and Tie-Point Ages in Core HH15-1252PC

Core depth (cm)	Lab code/Tie-point (TP)	Dated material	^{14}C age (years ± 2σ)	Calibrated age (years ± 2σ)	Reference
65	TP5		12,400 ± 150	13,811 ± 412	Jessen et al., 2010
120	TP6		12,700 ± 150	14,289 ± 508	Jessen et al., 2010
140	UBA-38275	Scaphopod	13,378 ± 49	15,280 ± 237	This work
145	UBA-38276	*N. pachyderma* sx.	14,806 ± 61	17,101 ± 244	This work
220	UBA-38822	*N. pachyderma* sx.	18,195 ± 90	21,074 ± 319	This work
260	TP7		19,710 ± 130	22,785 ± 341	Jessen et al., 2010
291	TP8		20,140 ± 130	23,320 ± 356	Jessen et al., 2010
306	TP9		22,900 ± 200	26,320 ± 477	Jessen et al., 2010
315	UBA-38823	*N. pachyderma* sx.	23,420 ± 129	26,786 ± 351	This work
460	UBA-38824	Bivalve	33,662 ± 362	37,652 ± 1,023	This work
495	UBA-42495	*N. pachyderma* sx.	26,360 ± 269	29,693 ± 547	This work[a]
590	UBA-41568	*N. pachyderma* sx.	36,514 ± 1,206	40,519 ± 1,696	This work

[a]Not used due too low carbon content.

3. Material and Methods

Piston core HH15-1252PC (79.04°N; 6.89°E) was retrieved from undisturbed contourite deposits north of Vestnesa Ridge, where no modern methane seepage occurs (Figure 1c). The 9.35 m long core was taken during a cruise with RV *Helmer Hanssen* in July 2015 from a water depth of 1,273 m (Figures 1a and 1c).

3.1. Core Handling and Sampling

The core was cut into 1-m sections, capped and taped at both ends, and stored at 4°C. Prior to opening, magnetic susceptibility was measured with a Bartington MS2 loop sensor. Thereafter the core sections were split longitudinally and the archive halves were X-rayed with a GEOTEK Multi Sensor Core Logger and color imaged with a Jai L-107CC 3 CCD RGB line scan camera installed on an Avaatech XRF.

The core was sampled in 1-cm-thick slices at 1–5 cm intervals. Samples were weighed, freeze-dried, and weighed again. They were subsequently wet-sieved over mesh-sizes 63, 100, and 500 μm. The residues were dried at 40°C and weighed and weight percent of each grain size was calculated.

3.2. AMS ^{14}C Dating

Seven AMS-^{14}C dates were performed on monospecific planktic foraminiferal samples and mollusks at the Chrono Centre of Queen's University, Belfast, Northern Ireland, UK) (Table 1). The radiocarbon dates were calibrated using the Marine20 calibration curve (Heaton et al., 2020) using CLAM 2.3.2. package in R software (Blaauw, 2010; Table 1).

3.3. Stable Isotope Analyses

Oxygen and carbon isotopes were measured on pristine tests of the benthic foraminiferal species *Cassidulina neoteretis* or *Melonis barleeanus* (150–250 μm size fraction; 31 overlapping samples), and planktic foraminiferal species *Neogloboquadrina pachyderma* (100–500 μm size fraction). We picked specimens with 4-chambers and avoided the largest and smallest tests within the 100–500 μm range. Up to 20 specimens of each species were analyzed on a Thermo Scientific MAT253 IRMS and Gasbench II at the Department of Geosciences, UiT the Arctic University of Norway, Tromsø, Norway. The analytical precision of the instrument is 0.1‰ for carbon and oxygen isotopes. The results are reported against the Vienna Peedee Belemnite

in-house standard. The $\delta^{18}O$ values of *M. barleeanus* were corrected by +0.4‰ to adjust for vital effects (Duplessy et al., 1980).

3.4. Element/Ca Analyses

For elemental analyses 10 to 30 pristine tests of *C. neoteretis* (150–250 μm size fraction), or *M. barleeanus* (150–350 μm size fraction), were picked and carefully crushed between two glass slides. *C. neoteretis*, the dominant benthic species in the record was selected. In some intervals, due to low occurrence of *C. neoteretis*, the second most common species *M. barleeanus* was measured ensuring overlap when possible. The samples were cleaned following the oxidative-reductive approach (Boyle & Keigwin, 1985/1986; Pena et al., 2005). The cleaning steps included removal of clay, reductive cleaning with hydrous hydrazine, oxidative cleaning with an alkali-buffered solution of hydrogen peroxide, and finally weak acid leaching. The samples were subsequently dissolved in HNO_3 (0.1 M) and analyzed using an inductively coupled plasma-optical emission spectrometer (Agilent 5100 ICP-OES) at the Department of Earth Sciences at the University of Cambridge, UK, to measure the $[Ca^{2+}]$. Samples were analyzed again at fixed $[Ca^{2+}]$ following the method of de Villiers et al. (2002), with concentrations ranging from 10 to 20 ppm of $[Ca^{2+}]$ used because of the small amount of material available for these samples. Two samples fell outside this range (8.8 and 9.2 ppm), but were retained in this investigation due to their consistency with the rest of the data set. Repeated measurements of an in-house standard solution with Mg/Ca of 1.46 mmol/mol showed a precision of 1.16% when run at a calcium concentration of 20 ppm during the analysis period, in comparison with a long-term precision of 0.53% for the same standard when run at a calcium concentration of 100 ppm over the 2-year period from July 2017 to July 2019.

Elemental ratios Mn/Ca, Fe/Ca, Al/Ca, and Na/Ca were used in combination to evaluate potential contamination. Thirteen samples were excluded because of indication of potential contamination shown by anomalously high values of Mn/Ca, Fe/Ca, Al/Ca, and Na/Ca (Table S1). The remaining samples showed small correlation between Mn/Ca, Fe/Ca, and Mg/Ca ($r^2 = 0.02$ for *C. neoteretis* and $r^2 = 0.34$ for *M. barleeanus* Mn/Ca-Mg/Ca; $r^2 = 0.08$ for *C. neoteretis* and $r^2 = 0.37$ for *M. barleeanus* Fe/Ca-Mg/Ca; Figure S2). Aluminum concentrations were under detection limits in 90% of the samples.

In order to obtain BWT changes, the Mg/Ca values were converted into temperature values using the calibration formulas from the Iceland shelf published by Kristjánsdóttir et al. (2007):

$$\mathrm{Mg/Ca}_{C.neoteretis} = 0.864 \pm 0.07 \times \exp\left(0.082 \pm 0.020 \times \mathrm{BWT}\right)$$

$$\mathrm{Mg/Ca}_{M.barleeanus} = 0.658 \pm 0.07 \times \exp\left(0.137 \pm 0.020 \times \mathrm{BWT}\right)$$

The data set of Kristjánsdóttir et al. (2007) comprise 10 surface samples containing living *C. neoteretis* and 31 samples of *M. barleeanus* from the Iceland shelf at water depths ranging from 211 to 637 m. Their Mg/Ca values range from 0.93 to 1.38 mmol/mol and 0.64 to 2.21 for *C. neoteretis* and *M. barleeanus*, respectively. Their BWT cover a temperature range from 0.19°C to 6.99°C. The equation from Barrientos et al. (2018) includes the *C. neoteretis* samples from Kristjánsdóttir et al. (2007) with the addition of 15 new core-top samples from the central Arctic Ocean. However, the calculated BWT based on our Mg/Ca data and the calibration formula by Barrientos et al. (2018) gave physically unrealistic values (down to −8.31°C; Figure S3). The calibration equation presented by Hansefrantz et al. (2018) for *M. barleeanus* and the equation presented in Sessford et al. (2018) for *C. neoteretis* do not change the reconstructed relative changes (Figure S3).

For *C. neoteretis*, the calibration of our Mg/Ca values based on the equation of Kristjánsdóttir et al. (2007) gave results of BWT varying from −1.78°C to 5.26°C downcore (ranging from 0.75 to 1.33 mmol/mol). One sample reached −2.36°C due to its low Mg/Ca (0.71 mmol/mol), however, it falls within the error of estimate of ±0.62°C of the calibration. For *M. barleeanus*, calibration based on the equation from Kristjánsdóttir et al. (2007) resulted in BWT estimates from −1.09°C to 2.99°C (Mg/Ca values range from 0.57 to 0.99 mmol/mol). The standard error of the estimate is ±1.1°C (Kristjánsdóttir et al., 2007).

We used the analytical error (±0.036 mmol/mol as 2 times the mean standard deviation) and the calibration errors from Kristjánsdóttir et al. (2007) to calculate the propagation error (calculated as the squared root

of the sum of the squared errors). Accordingly, the average of the estimated errors in BWT are ±1.03°C and ± 1.27°C for *C. neoteretis* and *M. barleeanus*, respectively.

3.5. Benthic Foraminiferal Analysis

Whenever possible, a total of >300 benthic foraminifera were counted from the 100–1,000 μm size fraction (the >500 μm fraction was dry-sieved with a 1-mm mesh size sieve). A total of 174 samples were counted of which 150 samples contained >300 specimens. Samples containing less than 100 specimens are considered to be nonrepresentative (Fatela & Taborda, 2002), but presented here when >50 specimens were counted. The foraminifera were identified to species level and relative abundance (%) calculated. The concentration (no. of tests/gram dry weight sediment) was also calculated.

3.6. Ice-Rafted Debris

IRD was counted on the >500 μm and the 150–500 μm size fractions, and the concentration of IRD grains per sample (no. of IRD/gram dry weight sediment) was calculated. To count IRD in the 150–500 μm size fraction, the 100–500 μm fraction was dry sieved using a 150-μm mesh-size sieve. Here, at least 300 mineral grains per sample were counted and the concentration calculated.

In order to differentiate the origin between sea ice and iceberg transported IRD, the grain-size ratio was calculated using the equation from Jessen and Rasmussen (2019):

$$\frac{(\text{no. of IRD} > 500\,\mu\text{m} \,/\, \text{no. of IRD}\, 150-500\,\mu\text{m})_{\text{sample}}}{(\text{no. of IRD} > 500\,\mu\text{m} \,/\, \text{no. of IRD}\, 150-500\,\mu\text{m})_{\text{average}}}$$

Although sea ice can transport any size of sediment grains, sea ice is more likely to transport fine-grained sediments (150–500 μm) compared to icebergs that can transport generally coarser material (Dowdeswell & Dowdeswell, 1989; Jessen & Rasmussen, 2019). Therefore, a grain-size ratio <1 would indicate a higher proportion of sea-ice transported grains, whereas a ratio >1 would indicate that IRD was likely transported by icebergs (Jessen & Rasmussen, 2019).

4. Results

4.1. AMS ^{14}C Dates

The calibrated ^{14}C dates and re-calibrated magnetic susceptibility tie-point dates (see Section 4.4. below) show that the age of the core for the interval between 5.46 and 0.65 m ranges from 40.5 to 13.8 ka (Table 1). The age at 4.95 m is considered too young and was discarded (Table 1). This is probably because the sample size was too low, which led to a too low content of graphite, increasing the impact of potential contamination with modern carbon (e.g., Gottschalk et al., 2018; Ruff et al., 2010).

4.2. Bottom Water Temperatures and Oxygen Isotopes

Mg/Ca values vary from 0.71 to 1.33 mmol/mol for *C. neoteretis* and from 0.56 to 0.99 mmol/mol for *M. barleeanus*. Using the calibrations of Kristjánsdóttir et al. (2007) and combining the records, BWT varies from −2.36°C to 5.26°C, and is 0.8°C in average (Figures 3 and 4). Seven samples of Mg/Ca were measured in both species and show that the difference in BWT calculated from the two species is 0.72°C ± 0.17°C.

The δ^{18}O of *C. neoteretis* δ^{18}O vary from 5.85‰ to 4.03‰ and *M. barleeanus* varies from 5.7‰ to 4.76‰. The values for the two species are in accordance for the upper 6.5 m (between 12 and 44 ka; Figure 4). Below 6.5 m (before 44 ka), both species show divergent δ^{18}O values and *M. barleenus* δ^{18}O remains generally higher with values ranging from 5.82‰ to 4.24‰ (Figure 4). In the upper part, the difference of δ^{18}O between *M. barleeanus* (after correction) and *C. neoteretis* (i.e., $\delta^{18}O_{M.\ barleeanus}$ minus $\delta^{18}O_{C.\ neoteretis}$) is 0.16 ± 0.03‰ ($n = 9$) and in the lower (below 6.50 m) 0.58 ± 0.07‰ ($n = 22$).

4.3. Benthic Foraminifera

Over 60 benthic foraminiferal species were identified in core HH15-1252PC. Almost 10% of the investigated samples contained less than 50 benthic foraminiferal specimens. The most abundant species is *C. neoteretis* (43% on average throughout the record and present in all samples except one), followed by *Cassidulina reniforme* and *M. barleeanus*. Other present species are *Astrononion gallowayi* and *Cibicides lobatulus* (presented together due to similar ecological preferences; Table 2), *Islandiella norcrossi, Elphidium* spp. (predominantly *E. excavatum*), *Nonionella* spp., and *Stainforthia* spp. Warm-water benthic species normally absent in the deep Nordic seas today include: *Bulimina costata*, *Sigmoilopsis schlumbergeri*, *Cibicidoides pachyderma*, *Gyroidina umbonata*, *Eggerella bradyi*, *Discospirina italica*, *Spirophthalmidium acutimargo*, *Sagraina subspinescens*, and *Anomalinoides minimus*. They have been grouped together as the "Atlantic species" group sensu (T. L. Rasmussen et al., 1996a). *Pyrgo serrata* has also been included in the group since it follows the distribution pattern of the other species. The group is restricted to a narrow horizon at 1.45–1.47 m (at ca. 17 ka) correlating with minimum $\delta^{18}O$ values (Figures 3 and 4). The ecological preferences of the most representative benthic foraminiferal species are given in Table 2.

4.4. Construction of the Age Model

The age-depth model of core HH15-1252PC was constructed using the planktic foraminiferal $\delta^{18}O$ record, supported by the magnetic susceptibility and the distribution of *C. neoteretis* (Figure 2). Marine isotope stage (MIS) 3 (from 9.1 m to 3.61 m depth in core) and MIS 2 (3.61 m to the top of the core) are identified by their characteristic planktic foraminiferal $\delta^{18}O$ (Figure 2). Additionally, the MIS 4/MIS 3 transition and early MIS 3 are characterized by high content of coarse IRD (Jessen et al., 2019) and the percentage of *C. neoteretis* exceeds 70% in MIS 2 (T. L. Rasmussen et al., 2014b; Sztybor & Rasmussen, 2017) and top MIS 4 (T. L. Rasmussen et al., 2014b) (Figure 3).

GI and GS events are recognized by correlating the planktic foraminiferal $\delta^{18}O$ to the $\delta^{18}O$ record in the North Greenland Ice Project (NGRIP) ice core with the GICC05modelext timescale b2k (= before 2 ka) (S.O. Rasmussen et al., 2014a; Svensson et al., 2008; Wolff et al., 2010). This relies on earlier results that show that low planktic $\delta^{18}O$ are caused by increased meltwater supply during GSs (e.g., Bond et al., 1993) (Figure 2). In addition, the distribution of the benthic foraminiferal species *C. neoteretis* follows the pattern of dominance of the polar planktic foraminiferal species *N. pachyderma* in modern settings (Lubinski et al., 2001; Polyak & Mikhailov, 1999). These species are most abundant in stadials in the North Atlantic and Nordic seas (e.g., Bond et al., 1993; T. L. Rasmussen & Thomsen, 2004). Therefore, the peaks of maximum percentages of *C. neoteretis* have been used here for further identification of stadial intervals (Figure 2). With this tuning to the ice core time scale, all ages are referring to b2k in the following.

The "24-ka event" (Jessen & Rasmussen, 2019) is a debris flow event followed by a pronounced deposition of IRD that occurred near-synchronously at the western Svalbard slope within a time interval of 500 years (Jessen et al., 2010). The lower boundary of the event at 2.92 m is coeval to the beginning of GI2/end of HS2. In order to reflect the rapid debris flow a tie-point was set 500 years earlier at the lower boundary of the event (22.84 ka at 2.65 m) (Figure 2).

The age model is also tested by the comparison of core HH15-1252PC to the magnetic susceptibility and planktic $\delta^{18}O$ of core JM11-19PC from the SE Norwegian Sea, which is independently tuned to the NGRIP ice core time scale (Ezat et al., 2014) (Figure 2). This core has been studied in great detail and includes well-described and well-dated tephra layers that can serve as direct tie-points to the NGRIP ice core (Davies et al., 2010, 2008; Ezat et al., 2014; Griggs et al., 2014; Wastegård & Rasmussen, 2014). The planktic $\delta^{18}O$ of both cores align and therefore strongly support our age-depth model (Figure S4).

In addition to AMS ^{14}C dates in core HH15-1252PC, magnetic susceptibility tie-points (TP5–TP9) are identified based on the reference magnetic susceptibility stack record for the western Svalbard slope (Jessen et al., 2010). The corresponding depths in the core and re-calibrated age for each tie-point are presented in Table 1. These dates are compared to the age-depth model in order to confirm the correlation between our sedimentary record and the ice core record. The age model curves are nearly parallel and the average difference between the estimated ages by the tuning to NGRIP and the calibrated ages is 509 ± 164 years (excluding the ^{14}C age at 4.95 m depth), which could be attributed to past changes in reservoir ages (Ezat

Table 2
Environmental Preference of Most Representative Benthic Foraminiferal Species in Core HH15-1252PC

Species	Environmental preference	Reference
Cassidulina neoteretis	Shallow infaunal. Cooled Atlantic origin waters with BWT from −1°C to 5.5°C (−1°C to 2°C in the slope). Found in organic-rich terrigenous fine-grained mud and responding to phytoplankton blooms. Present in seasonally ice-free sites and rare in permanently ice-covered areas.	Gooday & Lambshead, 1989; Jennings & Helgadottir, 1994; Kristjánsdóttir et al., 2007; Mackensen & Hald, 1988; Mackensen et al., 1985; Wollenburg & Kuhnt, 2000; Wollenburg & Mackensen, 1998
Melonis barleeanus	Deep to intermediate infaunal. Might migrate in the sediment column during times of food starvation. Feeds on altered organic detritus and it is related to high organic fluxes and stable primary productivity.	Caralp, 1989; Corliss, 1985; Linke & Lutze, 1993; Mackensen et al., 2000; Schönfeld, 2001; Wollenburg & Kuhnt, 2000
Cassidulina reniforme	Often in ice-distal glaciomarine environments. Prefers BWT <2°C and high food supply.	Hald & Korsun, 1997; Jernas et al., 2018; Mudie et al., 1984; Polyak et al., 2002; Steinsund, 1994
Astrononion gallowayi and Cibicidoides lobatulus	Occur in cold waters with coarse sediments and strong current activity.	Polyak et al., 2002; Sejrup et al., 1981; Steinsund, 1994; Wollenburg & Mackensen, 1998
Elphidium spp.	Sea-ice-edge related species. It can occur in varying and unstable conditions with low temperature and salinity and high turbidity.	Hald & Korsun, 1997; Korsun & Hald, 2000; Steinsund, 1994
Nonionella spp.	Indicator of high productivity areas. Feeds ion seasonally produced fresh phytodetritus, although it is capable of surviving prolonged starvation periods	Cedhagen, 1991; Gooday & Hughes, 2002; Korsun & Hald, 1998; Steinsund, 1994
Stainforthia spp.	Opportunistic species related to cold waters in high productivity areas covered seasonally by sea ice or areas where the sea ice margin is located. *S. fusiformis* and *S. feylingi* cope well with anoxic or low oxygen environments caused likely by high input of fresh food by algal blooms. *S. fusiformis* is also an indicator of rapidly changing environmental conditions	Alve, 1995, 2003; Hald & Korsun, 1997; Polyak et al., 2002; Seidenkrantz, 2013; Steinsund, 1994
"Atlantic species" group	Group consisting of species commonly found today at mid-latitudes in the North Atlantic and Mediterranean in BWT >2°C. Mainly phytodetritus species depending on pulsed food supply.	Rasmussen et al., 1996a, 1996b; Wollenburg & Mackensen, 1998; Wollenburg et al., 2004

et al., 2017b; Thornalley et al., 2015). This further validates our marine record-ice core synchronization (Figure 2). The sources of uncertainty in our age-depth model originate from (1) the uncertainties related to the identification of annual layers in NGRIP at GICC05modelext timescale (Svensson et al., 2016) and (2) the tuning between planktic foraminiferal $\delta^{18}O$ and the NGRIP $\delta^{18}O$. The core covers the end of MIS 4 to the end of MIS 2, from 63.8 to 12.9 ka.

5. Discussion

Together the planktic and benthic $\delta^{18}O$, IRD, BWT and benthic foraminiferal distribution patterns show clear millennial-scale variability (Figures 3 and 4). In general, low planktic and benthic $\delta^{18}O$ are linked to increases in BWT.

Benthic foraminiferal $\delta^{13}C$ have been widely used to track methane seepage from gas-influenced sediments by anomalously low $\delta^{13}C$ (e.g., Wefer et al., 1994). The $\delta^{13}C$ values of *C. neoteretis* and *M. barleeanus* range between −1.46‰ to −0.15‰ and −2.28‰ to −0.13‰ throughout the record, respectively. These values are within the range of "normal" carbon isotopes signatures for the species (Mackensen & Schmiedl, 2019; McCorkle et al., 1990) and therefore, the presence of methane affecting core HH15-1252PC can be excluded.

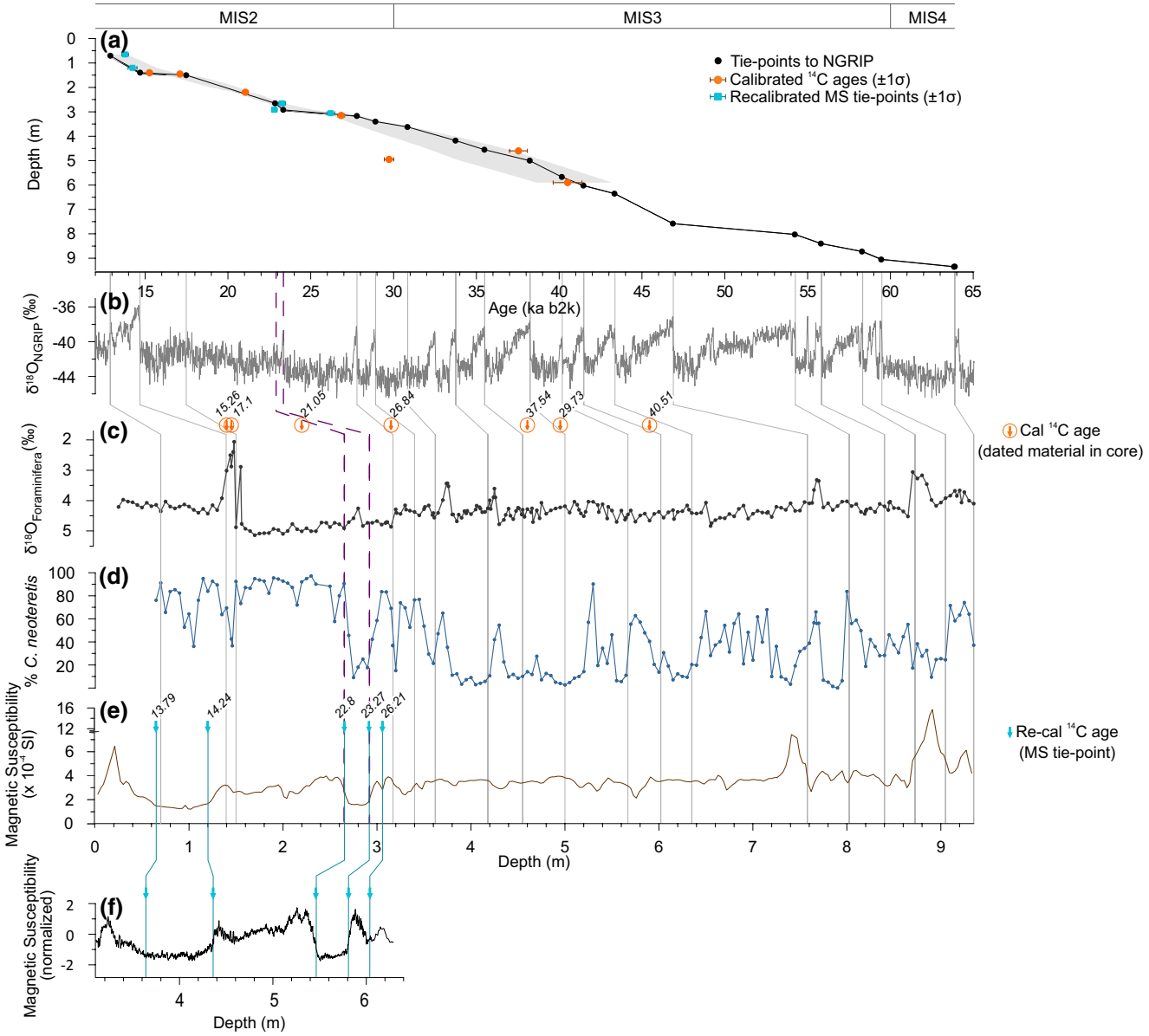

Figure 2. (a) Age-depth model of core HH15-1252PC constructed by correlating to (b) NGRIP ice-core with the GICC05modelext timescale (S.O. Rasmussen et al., 2014a; Svensson et al., 2008; Wolff et al., 2010). The shaded gray area in panel (a) shows the 95% confidence interval of the age-depth model with the calibrated radiocarbon ages. (c) $\delta^{18}O$ measured in planktic foraminiferal species *Neogloboquadrina pachyderma*. (d) Relative abundance of *Cassidulina neoteretis*. (e) Magnetic susceptibility of HH15-1252PC. (f) Magnetic susceptibility stack for the western Svalbard margin (Jessen et al., 2010). (e) Blue lines show the correlation between the magnetic susceptibility of core HH15-1252PC and (f) the western Svalbard magnetic susceptibility stack. (c–e) Gray lines indicate the correlation between core HH15-1252PC. Dashed purple lines show the upper and lower boundaries of the "24 ka event". Tie-point (TP) dates (blue vertical arrows) and calibrated ^{14}C dates performed in core HH15-1252PC (orange encircled vertical arrows) were used to confirm the tuning between our sediment core and NGRIP. Figure S4 shows the same data plotted against age.

5.1. Orbital Scale Changes

During the MIS 4/3 transition and early MIS 3 (64-55 ka), the content of coarse IRD deposited from icebergs increases (Figure 4). Benthic foraminiferal concentrations are generally low. *Cassidulina neoteretis* and *M. barleeanus* coexist in the interval, opposite to the rest of the record where they alternate in proportions, with *C. neoteretis* in general being the most abundant species of the two (Figure 3). In modern sediments at mid-depth on the slope of the Nordic Seas, *C. neoteretis* and *M. barleeanus* are some of the most common benthic foraminiferal species (Belanger & Streeter, 1980; Mackensen et al., 1985; Sejrup et al., 1981; Wollenburg &

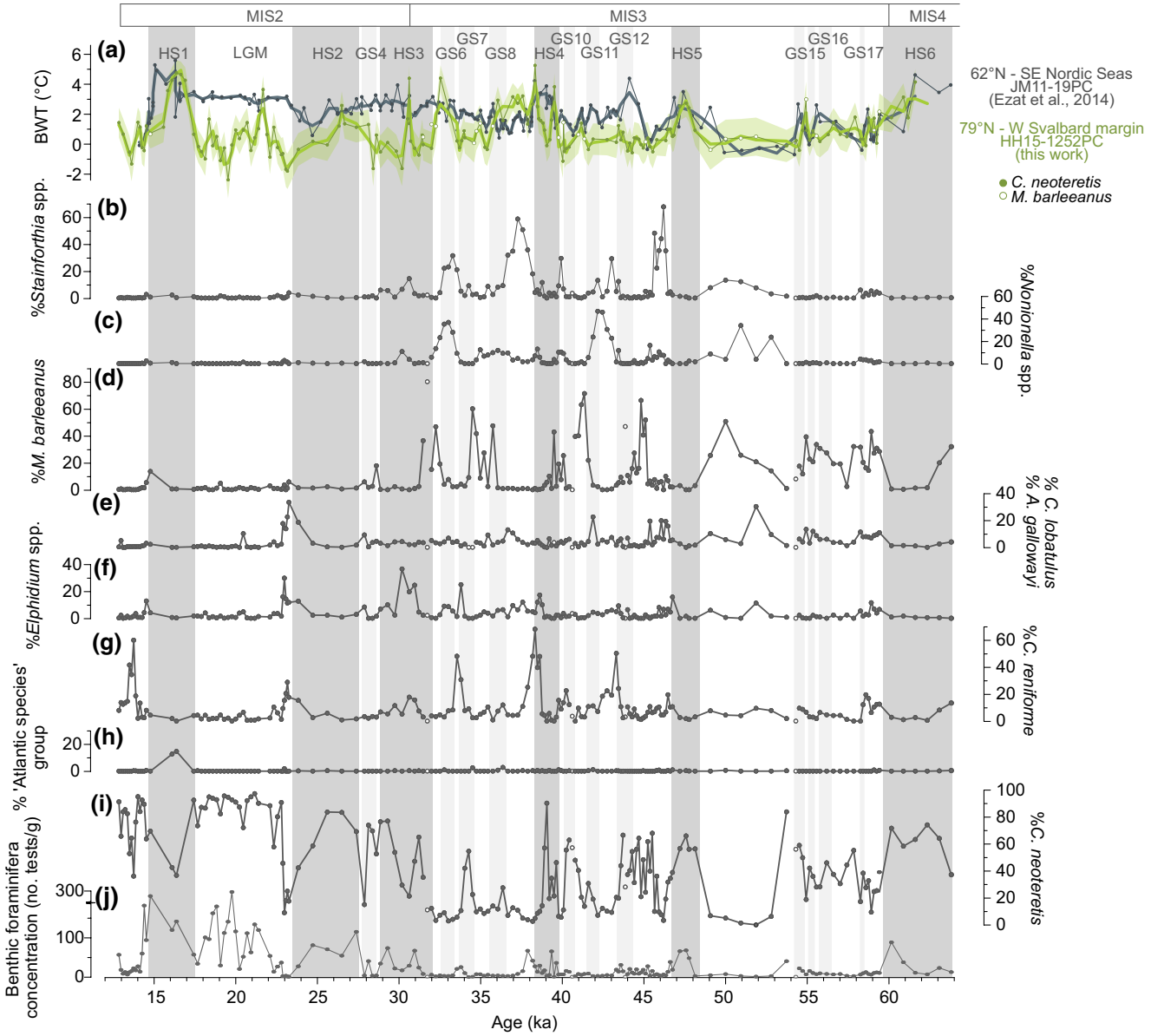

Figure 3. Records of core HH15-1252PC plotted versus GICC05modelext timescale (ka b2k; S.O. Rasmussen et al., 2014a; Svensson et al., 2008; Wolff et al., 2010). (a) Reconstructed bottom water temperature (BWT) from the northern Nordic Seas (core HH15-1252PC; this work) and southern Nordic Seas (JM11-19PC; Ezat et al., 2014). Light green shading indicates uncertainty interval calculated with error propagation in core HH15-1252PC. Thick line in both records shows smoothed records with Savitzky-Golay filtering. (b–i) Relative abundance of representative benthic foraminiferal species. (j) Concentration of benthic foraminiferal tests in number of specimens per g dry weight sediment. Open dots in (b–j) indicate samples with <50 benthic foraminifera per sample. Dark gray bands mark Heinrich Stadials (HS) and light gray bands Greenland Stadials (GS).

Mackensen, 1998). During early to mid MIS 3 (58-49 ka), the BWT remain relatively stable (except during GS and HS) with temperatures ca. 0.4°C for this period. The similarities between the benthic assemblage composition and the BWT with modern characteristics of the area indicate bottom water conditions similar to modern, with cold BWT implying deep convection (Figure 3). Planktic $\delta^{18}O$ show an increasing trend during MIS 3 (Figure 4).

A reduced Svalbard-Barents Sea Ice Sheet (SBIS) has been proposed for MIS 3 (Batchelor et al., 2019; Hughes et al., 2016; Jessen & Rasmussen, 2019). This is in agreement with the low concentration or absence of coarse IRD from mid to late MIS 3 (Figure 4). The grain-size ratio (<1) instead points to a higher abundance of rafted debris coming from sea ice. This is in accordance with the presence of benthic foraminiferal spe-

Figure 4. Records of core HH15-1252PC plotted versus with the GICC05modelext timescale (ka b2k; S.O. Rasmussen et al., 2014a; Svensson et al., 2008; Wolff et al., 2010). (a) Reconstructed bottom water temperature (BWT) (see text to Figure 3 for explanation). (b) Concentration of ice rafted debris (IRD) in number per gram dry weight sediment in 150–500 µm and >500 µm size fractions. (c) Grain-size ratio of IRD size fractions 150–500 µm/>500 µm; values > 1 indicate iceberg rafted debris and <1 indicate sea ice rafted debris (Jessen & Rasmussen, 2019). (d) $\delta^{13}C$ measured in benthic foraminiferal species *Cassidulina neoteretis* and *Melonis barleeanus* and planktic species *Neogloboquadrina pachyderma*. (e) $\delta^{18}O$ of the same species as in (d). Dark gray bands mark Heinrich Stadials (HS) and light gray bands Greenland Stadials (GS).

cies known to feed on phytodetritus (e.g., *Nonionella* spp., *Stainforthia* spp.) indicating presence of seasonal sea ice or the marginal ice zone (Figure 3 and Table 2).

During MIS 2 (30-11.7 ka), the concentration of coarse IRD is high compared to MIS 3 and planktic foraminiferal $\delta^{18}O$ are also high (Figure 4). Jessen and Rasmussen (2019) suggested an extensive SBIS based on high planktic foraminiferal $\delta^{18}O$, presence of allochthonous coarse IRD and absence of local IRD. Although the origin of the IRD is not investigated in this work, the proximity of the two study areas and the increased presence of medium to coarse sandy materials together with the high planktic $\delta^{18}O$ values during MIS 2 in core HH15-1252PC, also point to minimal local ice loss and an extensive SBIS. The BWT is variable throughout MIS 2, but remains within the limits of modern BWT at the study site, except for HS1, discussed further below. The dominance of *C. neoteretis* of high concentrations in MIS 2 indicates an amelioration of the oceanic conditions with an overall increased influence of AW in the study area and higher productivity (Seidenkrantz, 1995; Wollenburg et al., 2004) (Figure 3). This is further supported by the generally high concentrations of benthic foraminifera (up to ca. 300 tests/gram dry weight sediment during the LGM and late HS1).

During the last glacial maximum in MIS 2 (LGM; 24-19 ka) our core records variable BWT compared to the southern Nordic Seas (Ezat et al., 2014) (Figures 3, 4, and S4). The start of MIS 2, during HS2, in the western Svalbard margin is marked by a synchronous BWT decrease and high concentrations of coarse IRD indicating an increased production of icebergs related to the growth of the SBIS or a re-activation of

ice-streams (Jessen et al., 2010; Winsborrow et al., 2010) (Figure 4). This event also correlates to an event of anomalously low magnetic susceptibility around 24 ka BP (the "24-ka mass transport/IRD event" of Jessen & Rasmussen, 2019; see also above) and occurring at the end of HS2/beginning of GI2 (Jessen & Rasmussen, 2019; Jessen et al., 2010; T. L. Rasmussen et al., 2007). In core HH15-1252PC, the concentration of benthic foraminifera is low and species related to coarser sediments and stronger current activity such as *A. gallowayi* and *C. lobatulus* occur (Figure 3 and Table 2). Evidence of a similar mass transport event with similar timing is found all along the northwestern Barents Sea (Jessen & Rasmussen, 2019; Jessen et al., 2010; Laberg & Vorren, 1995; Vorren et al., 1998) and reaching to the Yermak Plateau (Chauhan et al., 2014; Howe et al., 2007). Jessen and Rasmussen (2019) interpret this event as increased slope instability and iceberg calving and thinning of the ice-sheet as it reached the shelf break.

Debris flow events could have entrained fresh cold shelf water via a hyperpycnal flow into the deepest basins (Stanford et al., 2011). The high benthic $\delta^{13}C$ (up to −0.15‰) observed contemporaneously with the debris flow event could reflect the input of well-ventilated shelf waters and the generally high benthic $\delta^{18}O$ (ca 5.7‰) are indicative of the cold BWT. Another hypothesis to explain the low temperatures during this interval involves dense cold brines (high benthic $\delta^{18}O$ and $\delta^{13}C$; Mackensen et al., 2016; T. L. Rasmussen & Thomsen, 2009) formed on the shelf of Spitsbergen and reaching the study area. The low abundance of benthic foraminifera in this interval could be due to the corrosive nature of brines (e.g., Fossile et al., 2020) (Figure 3j). In addition, the increased relative abundances of the typical interstadial species *C. reniforme, C. lobatulus*, and *A. gallowayi* and decrease in % *C. neoteretis* (e.g., T. L. Rasmussen et al., 2014b; see also Section 5.2.1. below) confirm the presence of relatively cold saline waters (Steinsund, 1994) and precludes downtransportation of specimens. Knies et al. (2018) suggested the existence of a large polynya in front of the SBIS caused by strong easterly katabatic winds and a strong polar front pushing the sea ice eastwards during the LGM period (27-19.5 ka). This scenario could facilitate the formation of seasonal sea ice and brine rejection, and consequently the formation of a very dense cold, water mass formed in the coastal area and flowing downslope to our core site (Figure 5b).

5.2. Millennial-Scale Paleoceanographic Changes

5.2.1. Greenland Interstadials

In Greenland ice cores, interstadials are characterized by a short-lasting peak in maximum temperature followed by gradual cooling (Johnsen et al., 1992, 2001; Kindler et al., 2014). In core HH15-1252PC the end of stadials and beginning of interstadials, the % *Elphidium* spp. seems to increase followed by increase in % *C. reniforme* (most clearly seen in the transitions HS4–GI12, GS12–GI11, and GS7–GI6; Figure 3). In these environments, a replacement of *Elphidium* spp. by *C. reniforme* is interpreted as ameliorated conditions by increased primary production after a melting event (Korsun & Hald, 1998). Early during the GIs, the appearance and subsequent decrease of coarser IRD is also indicative of increased calving and melting due to the sea surface and atmospheric warming (Jessen & Rasmussen, 2019; T. L. Rasmussen & Thomsen, 2013) (Figures 3 and 5).

In the mid-late part of some interstadials, the phytodetritus species *Stainforthia* spp. and *Nonionella* spp. become dominant, particularly during MIS 3 (Figure 3). Their presence indicate that the core site must have been under the influence of the high-productivity zones of the marginal ice zone with increased seasonal sea-ice cover (Polyak et al., 2013; Figure 5). The relative dominance in the foraminiferal assemblages of *M. barleeanus* demonstrate the establishment of high and stable productivity during some of these interstadial periods (Wollenburg et al., 2001) (Table 2 and Figure 3). The intervals with dominance of *M. barleeanus*, *Nonionella* spp., and *Stainforthia* spp. are characterized by dissolution and a high degree of fragmentation and low concentrations and flux of faunas as recorded in nearby cores JM05-31GC, JM10-335GC, and JM10-333GC (T. L. Rasmussen et al., 2014b; Sztybor & Rasmussen, 2017) (Figure S1). The high productivity in late interstadials indicated by the composition of the benthic faunas, but with low concentrations is probably caused by the high accumulation rates of organic carbon that could cause dissolution of calcareous specimens (Wollenburg et al., 2004).

Our benthic foraminiferal data and succession of species in the GIs are supported by sea-ice studies in the southern Nordic Seas (Hoff et al., 2016; Wary et al., 2017). A high-resolution study of four D-O events in a

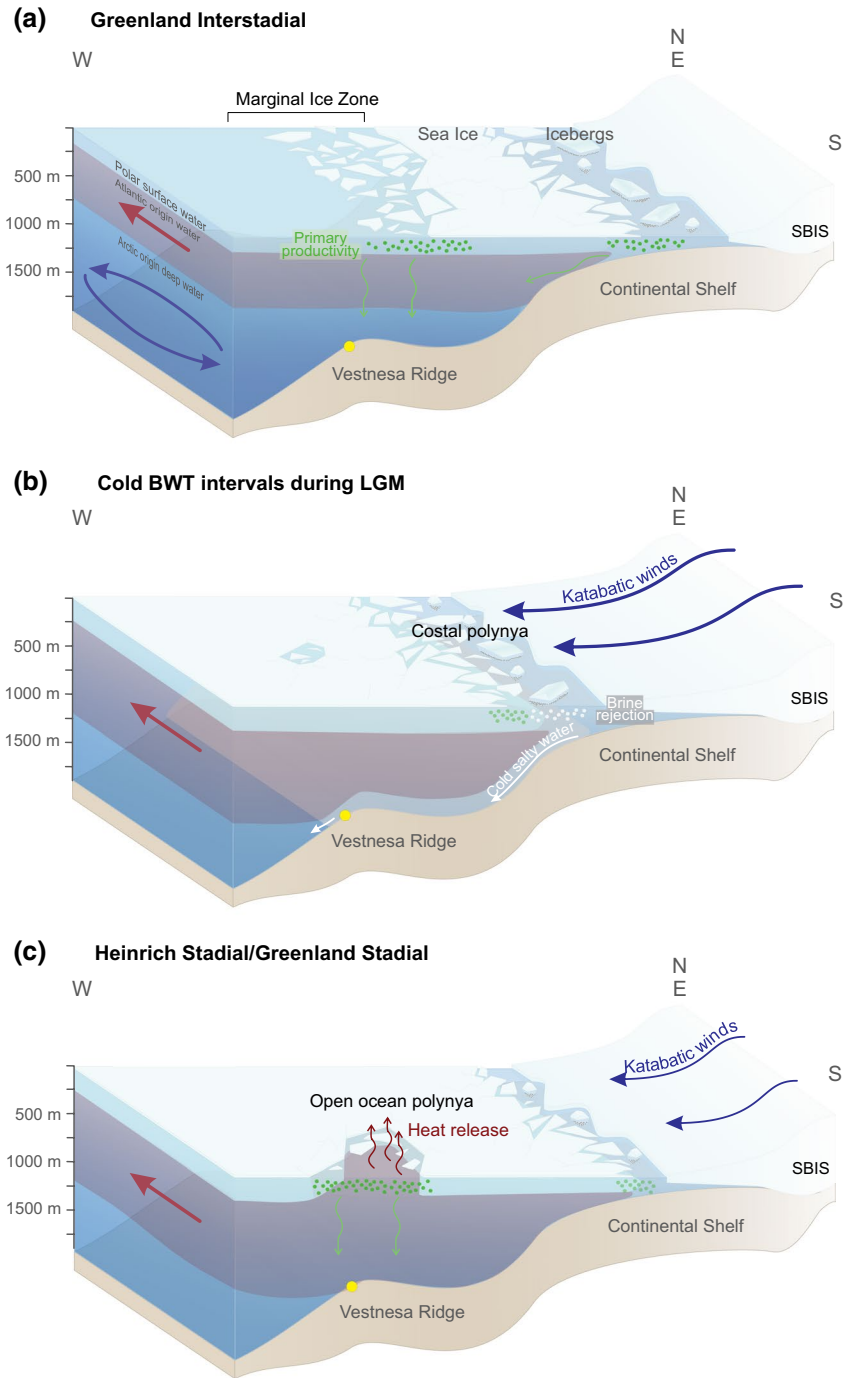

Figure 5. Schematic diagrams showing interpretations of paleoenvironments for (a) Greenland Interstadials, (b) last glacial maximum (LGM), and (c) Heinrich Stadials. Yellow dot shows location of core HH15-1252PC. Abbreviation: SBIS, Svalbard-Barents Sea Ice Sheet.

nearby core have confirmed this result (Sadatzki et al., 2019). Hoff et al. (2016) showed that sea-ice cover decreases abruptly at the start of GIs causing open ocean conditions and phytoplankton blooms. Sadatzki et al. (2019) also suggested that the most extensive open-ocean conditions coincided with the initial GI warming. Highest benthic foraminiferal concentrations occur late in the GS and at the beginning of GIs corresponding to the early GI phytoplankton blooms. By the mid-late GI, concentrations drop abruptly and species with an affinity to conditions at the sea-ice margin increase in relative abundance, as a sign of

the re-growth of sea ice during the interstadial cooling phase (Hoff et al., 2016; T. L. Rasmussen & Thomsen, 2004; Figures 3 and 5). Higher amounts of sea-ice related IRD support the presence of sea ice during these intervals (Figure 4).

Well within the GI, the lowest benthic foraminiferal concentrations coincide with the appearance of *C. lobatulus* and *A. gallowayi* and decrease/disappearance of the phytodetritus related species, indicating stronger bottom current activity (Figure 3). T. L. Rasmussen and Thomsen (2004) suggested that the interstadial oceanic setting was similar to modern conditions, with surface water of Atlantic origin flowing northwards in the Nordic Seas, overlaying a cold deep water created by winter convection. BWT seems to stabilize and be relatively lower than during the related stadial interval, confirming the presence of cooler waters in the area (Figures 3 and 4). In the southern Nordic Seas lower BWTs are also observed during interstadials (Ezat et al., 2014; Sessford et al., 2018, 2019). The strength of the convection decreases during the interstadial cold phase toward the onset of a GS (T. L. Rasmussen & Thomsen, 2004) (Figure 3).

5.2.2. Heinrich Stadials and Greenland Stadials

Both planktic and benthic foraminifera show low $\delta^{18}O$ values during stadials compared to the preceding interstadials (Figure 4). The most pronounced planktic $\delta^{18}O$ decreases occur during HSs in a time window of 1–2 Kyr (e.g., down to 2.06‰ and 3.35‰ during HS1 and HS5, respectively; Figure 3). Benthic $\delta^{18}O$ decreases within the intervals with the lowest planktic $\delta^{18}O$, together with the increase in BWT. Most of the decreases in benthic $\delta^{18}O$ can be explained by the increase in BWT (T. L. Rasmussen & Thomsen, 2004). This is indicated by calculation of local seawater $\delta^{18}O$ based on the combination of the stable isotope values and BWTs in core HH15-1252PC (Text S1 and Figure S5). The low planktic $\delta^{18}O$ has been attributed to low subsurface salinity due to the presence of polar meltwater from melting icebergs causing surface stratification (e.g., Bond et al., 1993) (here originating from the SBIS [e.g., Lekens et al., 2006]).

Environmental conditions with a persistent sea-ice cover, surface stratification due to presence of cold, polar meltwater insulating the AW from the atmosphere cause a decrease in paleoproductivity as seen in the Arctic Ocean today (Wollenburg et al., 2001). This is also indicated by the reduced concentration of the benthic foraminiferal faunas during HSs (Figures 3 and 5). Preservation of foraminifera in GS and HS events are excellent with low fragmentation (T. L. Rasmussen et al., 1996a, 1996b, 2014b). *Cassidulina neoteretis* is almost the only benthic foraminifera present (>70%), indicating at least temporarily ice-free conditions. Localized ice-free areas in a perennially sea-ice covered ocean can be explained by the development of polynyas (Figure 5). These could be caused by intermittent resurfacing of subsurface Atlantic warm and salty waters. Phytoplankton blooms in polynyas could allow the development of a benthic foraminiferal fauna, shown here by the gradually increasing benthic foraminiferal concentrations following BWT maxima (Figure 3).

The highest BWT occur during GSs, with maxima during most HSs, when temperature rises to between 2°C and 5°C (Figures 3 and 4). Greenland stadials GS6, GS8, and GS15 show similar trends, but the warming signals are most consistent during HSs. BWT increases related to HSs have been observed in the northwestern Atlantic and southern Nordic Seas (Ezat et al., 2014; Marcott et al., 2011; T. L. Rasmussen & Thomsen, 2004; T. L. Rasmussen et al., 1996b). At Vestnesa Ridge methane seep sites, the presence of vesicomyid/solemyid bivalves at HS1 has also been suggested as the result of higher BWT (Hansen et al., 2020; Sztybor & Rasmussen, 2017; Thomsen et al., 2019). In our core, the relative abundance of the "Atlantic species" group is high in HS1 (ca. 20% of the assemblage) indicating higher BWTs (Table 2), confirmed by our high Mg/Ca (BWT up to 5°C) (Figure 3). In other cores from the Nordic Seas and North Atlantic Ocean, the group occur during several HS and GS events indicting increased BWT (e.g., Chauhan et al., 2016; Danielsen, 2017; Ezat et al., 2014; Jansen et al., 1983; T. L. Rasmussen & Thomsen, 2004, 2017; T. L. Rasmussen et al., 1996a, 1996b, 2007, 2014b; Wollenburg et al., 2004) (Figure 6). Together with *C. neoteretis* that responds to a number of environmental parameters including higher temperatures, the benthic faunas together generally indicate warmer bottom waters during stadial events (see e.g., Jennings & Helgadottir, 1994; Jennings et al., 2004; Lubinski et al., 2001).

The warming during HSs in the Nordic Seas has previously been explained by the thickening and deepening of the AW down to at least 1,750 m in the absence/reduction of deep water formation (Ezat et al., 2014; T. L. Rasmussen & Thomsen, 2004; T. L. Rasmussen et al., 1996a, 1996b). During GSs and HSs the southeastern

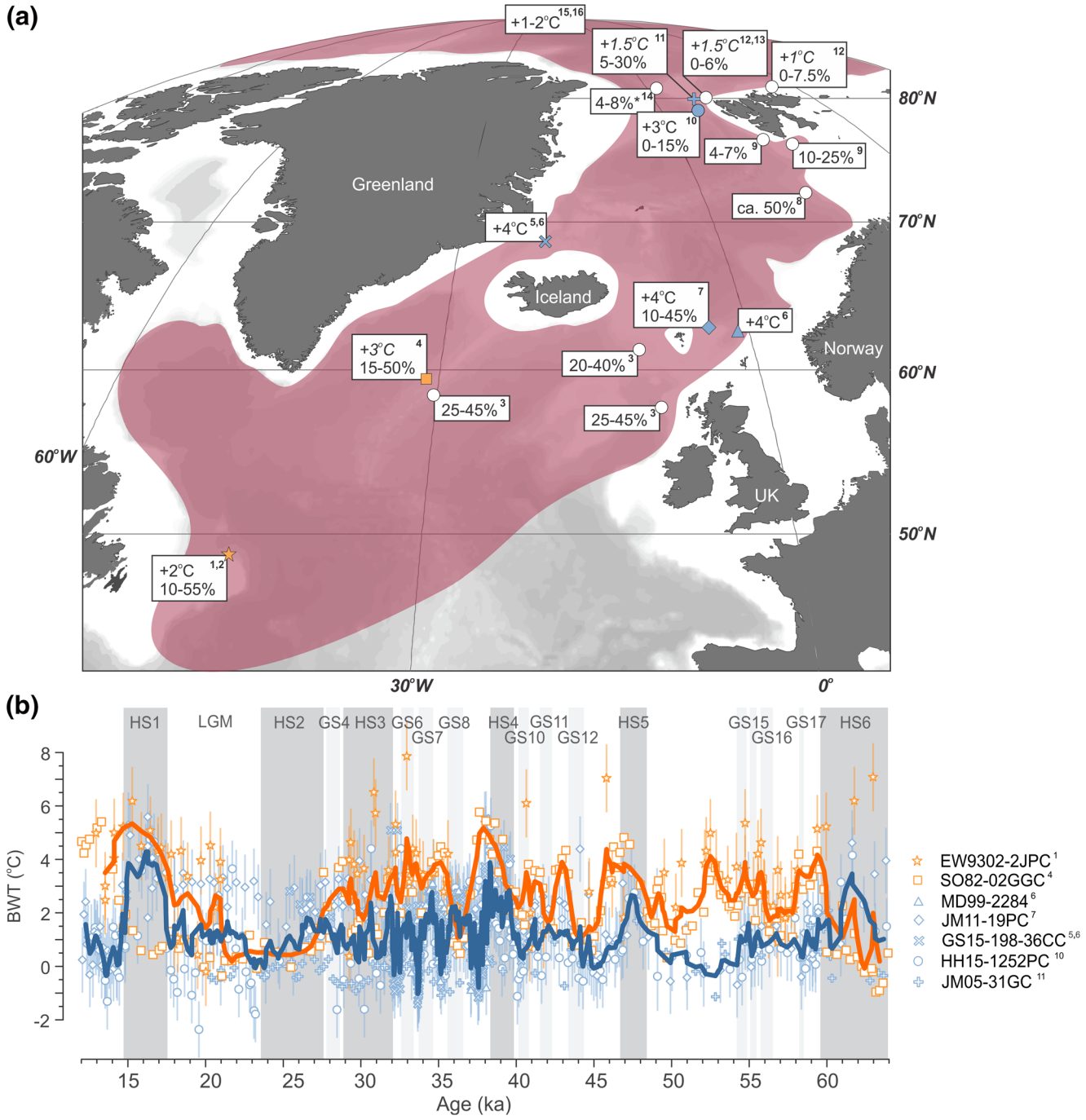

Figure 6. (a) Compilation of core records from the northern North Atlantic Ocean, Nordic Seas, and Arctic Ocean containing the "Atlantic species" group (in percentage; sensu Rasmussen et al. (1996a), except for core no. 13, where the Atlantic species group follows the definition of Wollenburg et al. [2004]) and absolute bottom water temperatures (BWT) (°C) increases during Heinrich Stadials and Greenland Stadials. BWT increases were calculated as difference to the previous interstadial period. BWT given in italics were obtained from benthic foraminiferal transfer functions. Colored area indicates northward Atlantic subsurface intermediate water flow. (b) BWT records compilation for the last 64 ka for water depths between 800 and 1,500 m. Smoothed lines were obtained with five point weighted average. Symbols (orange for the North Atlantic and blue for the Nordic Seas) are the same as in panel (a) to identify each specific core location. References: 1 = Marcott et al. (2011); 2 = T. L. Rasmussen et al. (2003); 3 = T. L. Rasmussen & Thomsen (2004); 4 = T. L. Rasmussen & Thomsen (2017); 5 = Sessford et al. (2018); 6 = Sessford et al. (2019); 7 = Ezat et al. (2014); 8 = Danielsen (2017); 9 = T. L. Rasmussen et al. (2007); 10 = This work; 11 = T. L. Rasmussen et al. (2014b); 12 = Chauhan et al. (2016); 13 = Chauhan et al. (2014); 14 = Wollenburg et al. (2004); 15 = Cronin et al. (2012); 16 = Cronin et al. (2017).

Nordic Seas were persistently covered by (nearly) perennial sea ice during GSs and HSs for the last 90 ka (Hoff et al., 2016). Results from the LGM of nearby core MSM5/5-712-2 from the eastern Fram Strait (Figure S1) showed almost full sea-ice cover (Müller & Stein, 2014) and therefore the Fram Strait probably also was sea-ice covered during earlier GS and HS. A strong halocline (T. L. Rasmussen & Thomsen, 2004; Wary et al., 2017), and extended sea-ice cover would permit the subduction and advection of warm subsurface AWs without losing heat. The stratification would be more pronounced during HSs than during GSs as indicated by the low planktic foraminiferal $\delta^{18}O$, and leading to warmer BWT during HSs than during GS. Another potential cause of the warming of the intermediate water depths are the lower sea level and smaller continental shelf during these periods (Cronin et al., 2012). The subduction of the AW below a stronger halocline occurs today in the northern Fram Strait. There the AW becomes an intermediate water mass, being insulated from the atmosphere below the cold, low-saline polar surface water and cooling only ca. 2°C from the moment it enters the Arctic Ocean through the Fram Strait until it reaches the Chuckchi Sea (Rudels et al., 2004).

A previous reconstruction of BWT based on transfer functions of benthic foraminiferal faunas (i.e., based on an average of the whole assemblage) records a BWT increase of up to 3°C during HSs in the southern Yermak Plateau at ca. 800 m water depth (T. L. Rasmussen et al.,2014b). In the central-northwestern Barents Sea between 448 and 785 m water depth, BWT up to 1.5°C were reconstructed using benthic foraminiferal transfer functions (Chauhan et al., 2014, 2016). During HSs in the North Atlantic and SE Nordic Seas at water depths between 1,200 and 1,500 m, BWT increased to 5.5°C (Ezat et al., 2014; Marcott et al., 2011; Sessford et al., 2018, 2019) and in the Fram Strait our results show a temperature increase to 5°C, based on benthic foraminiferal Mg/Ca (Figure 6). This indicates a minimal heat loss in the Nordic Seas, probably due to the insulation of the subsurface below the strong halocline. In the Arctic Ocean, between 800 and 1,500 m water depth the benthic ostracod Mg/Ca indicated a temperature increase between 1°C and 2°C during the same periods (Cronin et al., 2012, 2017).

The warming at intermediate water depths is therefore consistent from the North Atlantic Ocean from 45°N (Marcott et al., 2011) into the Nordic Seas at 62°N (Ezat et al., 2014) and through the Fram Strait at 79°N (this study) to the Chukchi Sea (Cronin et al., 2012) (Figure 6). Such an extensive heat reservoir would have contributed significantly to the melting of the sea ice and atmospheric heating at the end of the GS and HS events and beginning of GI events. Toward the end of this long period of stratification, the supply of icebergs and meltwater probably declined, leading to increased density in the surface waters until surface and subsurface water densities were similar enough to allow for mixing. This is supported by the model experiment performed by Jensen et al. (2016), who showed that both the decrease of freshwater input and the increase of subsurface temperatures could trigger instability and disappearance of sea ice. According to Cronin et al. (2012) in the Arctic Ocean during stadial conditions, the reduced hydrological cycle and subsequent decrease in river discharge could have major effects in shallowing of the halocline and increase in surface salinity. In a sea-ice free ocean the AW could resurface releasing the accumulated heat from the ocean to the atmosphere. Due to its high salinity, the cooling of this water mass at its contact with the atmosphere could also reactivate the convection in the Nordic Seas, contributing to the formation of NADW, as in the modern Nordic Seas. With a strengthened thermohaline circulation heat would be transported back to northern latitudes at the surface. Although the onset of the abrupt interstadial warming must have involved complex atmosphere-cryosphere-ocean-se- ice interactions (e.g., Li & Born, 2019; Sheriff-Tadano & Abe-Ouchi, 2020), our compilation of BWT records (Figure 6) highlights the importance of a vast subsurface heat reservoir from 45°N to the Chuckchi Sea in driving these rapid events.

6. Summary and Conclusions

We have studied piston core HH15-1252PC from 1,273 m water depth north of Vestnesa Ridge at 79°N in the eastern Fram Strait for the reconstruction of water mass exchange through the Fram Strait and the evolution of convection in the Nordic Seas in relation to abrupt climate oscillations. Combined Mg/Ca measurements, stable isotopes, benthic foraminiferal fauna analysis and grain-size distribution and deposition of IRD, showed distinct paleoceanographic patterns that align with GI and GS (particularly HSs) in the northern Nordic Seas during the last glacial period.

GIs followed the previously suggested evolution, with oceanographic settings similar to modern with the presence of cold bottom water and deep convection. The occurrence of phytodetritus species suggest seasonal or temporary sea-ice cover in the area, leading to high productivity. The last glacial maximum (24-19 ka) showed large variations in BWT, probably related to the dynamics of the SBIS during that period.

HSs showed increases in BWT of up to 5°C due to the subduction of the AW masses beneath a fresh surface water layer and a strong halocline and stop or near-stop in deep convection. The development of *Cassidulina neoteretis* during these intervals with extensive sea-ice cover could be the result of open ocean polynyas caused by short episodes of resurfacing of the warm Atlantic origin waters, which would allow some food supply to the deep ocean.

Our results are in agreement with previously published work in the northern North Atlantic, southern Nordic Seas and Arctic Ocean, where a warm AW mass occupied the intermediate water depths below a strong halocline during HSs stretching from 45°N in the North Atlantic Ocean into the Nordic Seas to 79°N and to the Chukchi Sea in the Arctic Ocean. The resurfacing of this vast heat reservoir of AW during HSs caused release of heat to the atmosphere that preconditioned the ocean to the onset of convection and a new GI. This work highlights the important role of the oceanographic changes in the high latitude North Atlantic for the development of GI-GS cycles.

Data Availability Statement

The data from this paper is available at PANGAEA database: https://doi.pangaea.de/10.1594/PANGAEA.925428.

Acknowledgments
We thank the captain and crew of RV Helmer Hansen and the participants of cruise GEO8144/3144 for their assistance in the core retrieval. We are grateful to Matteus Lindgren (Department of Geosciences, UiT—The Arctic University of Norway) who performed stable isotope measurements. We thank Luke Skinner for helpful discussions. We thank J. Farmer and an anonymous reviewer for greatly improving this manuscript with their helpful and constructive comments. This research was supported by CAGE (Centre for Arctic Gas Hydrate, Environment and Climate) funded by the Research Council of Norway through its Centers of Excellence funding scheme, grant number 223259. N. El bani Altuna wants to thank the Cushman Foundation for Foraminiferal Research for the Student Research Award, which supported the expenses of Mg/Ca analyses. M. M. Ezat is funded by the Research Council of Norway and the Co-funding of Regional, National, and International Programmes (COFUND)—Marie Skłodowska-Curie Actions under the EU Seventh Framework Programme (FP7), project number 274429.

References

Aagaard, K., & Coachman, L. K. (1968). The East Greenland Current north of Denmark Strait: Part I. *Arctic*, *21*, 181–200. https://doi.org/10.14430/arctic3262

Aagaard, K., Coachman, L. K., & Carmack, E. (1981). On the halocline of the Arctic Ocean. *Deep Sea Research Part A. Oceanographic Research Papers*, *28*(6), 529–545. https://doi.org/10.1016/0198-0149(81)90115-1

Alve, E. (1995). Benthic foraminiferal distribution and recolonization of formerly anoxic environments in Drammensfjord, southern Norway. *Marine Micropaleontology*, *25*(2–3), 169–186. https://doi.org/10.1016/0377-8398(95)00007-n

Alve, E. (2003). A common opportunistic foraminiferal species as an indicator of rapidly changing conditions in a range of environments. *Estuarine, Coastal and Shelf Science*, *57*(3), 501–514. https://doi.org/10.1016/s0272-7714(02)00383-9

Barrientos, N., Lear, C. H., Jakobsson, M., Stranne, C., O'Regan, M., Cronin, T. M., et al. (2018). Arctic Ocean benthic foraminifera Mg/Ca ratios and global Mg/Ca-temperature calibrations: New constraints at low temperatures. *Geochimica et Cosmochimica Acta*, *236*, 240–259. https://doi.org/10.1016/j.gca.2018.02.036

Batchelor, C. L., Margold, M., Krapp, M., Murton, D. K., Dalton, A. S., Gibbard, P. L., et al. (2019). The configuration of Northern Hemisphere ice sheets through the Quaternary. *Nature Communications*, *10*(1), 3713. https://doi.org/10.1038/s41467-019-11601-2

Belanger, P. E., & Streeter, S. S. (1980). Distribution and ecology of benthic foraminifera in the Norwegian-Greenland Sea. *Marine Micropaleontology*, *5*, 401–428. https://doi.org/10.1016/0377-8398(80)90020-1

Blaauw, M. (2010). Methods and code for 'classical' age-modelling of radiocarbon sequences. *Quaternary Geochronology*, *5*(5), 512–518. https://doi.org/10.1016/j.quageo.2010.01.002

Bond, G. C., Broecker, W., Johnsen, S., McManus, J., Labeyrie, L., Jouzel, J., & Bonani, G. (1993). Correlations between climate records from North Atlantic sediments and Greenland ice. *Nature*, *365*(6442), 143–147. https://doi.org/10.1038/365143a0

Bond, G. C., & Lotti, R. (1995). Iceberg discharges into the North Atlantic on millennial time scales during the last glaciation. *Science*, *267*(5200), 1005–1010. https://doi.org/10.1126/science.267.5200.1005

Boyle, E. A., & Keigwin, L. D. (1985). Comparison of Atlantic and Pacific paleochemical records for the last 215,000 years: Changes in deep ocean circulation and chemical inventories. *Earth and Planetary Science Letters*, *76*(1–2), 135–150. https://doi.org/10.1016/0012-821x(85)90154-2

Brady, E. C., & Otto-Bliesner, B. L. (2011). The role of meltwater-induced subsurface ocean warming in regulating the Atlantic meridional overturning in glacial climate simulations. *Climate Dynamics*, *37*(7–8), 1517–1532. https://doi.org/10.1007/s00382-010-0925-9

Bünz, S., Polyanov, S., Vadakkepuliyambatta, S., Consolaro, C., & Mienert, J. (2012). Active gas venting through hydrate-bearing sediments on the Vestnesa Ridge, offshore W-Svalbard. *Marine Geology*, *332*, 189–197. https://doi.org/10.1016/j.margeo.2012.09.012

Caralp, M. H. (1989). Abundance of *Bulimina exilis* and *Melonis barleeanum*: Relationship to the quality of marine organic matter. *Geo-Marine Letters*, *9*(1), 37–43. https://doi.org/10.1007/bf02262816

Cedhagen, T. (1991). Retention of chloroplasts and bathymetric distribution in the sublittoral foraminiferan *Nonionellina labradorica*. *Ophelia*, *33*(1), 17–30. https://doi.org/10.1080/00785326.1991.10429739

Chauhan, T., Rasmussen, T. L., & Noormets, R. (2016). Palaeoceanography of the Barents Sea continental margin, north of Nordaustlandet, Svalbard, during the last 74 ka. *Boreas*, *45*(1), 76–99. https://doi.org/10.1111/bor.12135

Chauhan, T., Rasmussen, T. L., Noormets, R., Jakobsson, M., & Hogan, K. A. (2014). Glacial history and paleoceanography of the southern Yermak Plateau since 132 ka BP. *Quaternary Science Reviews*, *92*, 155–169. https://doi.org/10.1016/j.quascirev.2013.10.023

Corliss, B. H. (1985). Microhabitats of benthic foraminifera within deep-sea sediments. *Nature*, *314*(6010), 435–438. https://doi.org/10.1038/314435a0

Cronin, T. M., Dwyer, G. S., Caverly, E. K., Farmer, J., DeNinno, L. H., Rodriguez-Lazaro, J., & Gemery, L. (2017). Enhanced Arctic amplification began at the Mid-Brunhes Event~ 400,000 years ago. *Scientific Reports*, *7*(1), 1–7. https://doi.org/10.1038/s41598-017-13821-2

Cronin, T. M., Dwyer, G. S., Farmer, J., Bauch, H. A., Spielhagen, R. F., Jakobsson, M., et al. (2012). Deep Arctic Ocean warming during the last glacial cycle. *Nature Geoscience*, *5*(9), 631–634. https://doi.org/10.1038/ngeo1557

Danielsen, I. K. (2017). Paleoceanographic development during the last deglaciation and Holocene, over the Bear Island slide scar, SW Barents Sea (Master's thesis). UiT Norges arktiske universitet. Retrieved from https://munin.uit.no/bitstream/handle/10037/10615/thesis.pdf?sequence=2isAllowed=y

Dansgaard, W., Clausen, H. B., Gundestrup, N., Hammer, C. U., Johnsen, S. F., Kristinsdottir, P. M., & Reeh, N. (1982). A new Greenland deep ice core. *Science*, *218*(4579), 1273–1277. https://doi.org/10.1126/science.218.4579.1273

Dansgaard, W., Johnsen, S. J., Clausen, H. B., Dahl-Jensen, D., Gundestrup, N. S., Hammer, C. U., et al. (1993). Evidence for general instability of past climate from a 250-kyr ice-core record. *Nature*, *364*(6434), 218–220. https://doi.org/10.1038/364218a0

Davies, S. M., Wastegård, S., Abbott, P. M., Barbante, C., Bigler, M., Johnsen, S. J., et al. (2010). Tracing volcanic events in the NGRIP ice-core and synchronising North Atlantic marine records during the last glacial period. *Earth and Planetary Science Letters*, *294*(1–2), 69–79. https://doi.org/10.1016/j.epsl.2010.03.004

Davies, S. M., Wastegård, S., Rasmussen, T. L., Svensson, A., Johnsen, S. J., Steffensen, J. P., & Andersen, K. K. (2008). Identification of the Fugloyarbanki tephra in the NGRIP ice core: A key tie-point for marine and ice-core sequences during the last glacial period. *Journal of Quaternary Science*, *23*(5), 409–414. https://doi.org/10.1002/jqs.1182

de Villiers, S., Greaves, M., & Elderfield, H. (2002). An intensity ratio calibration method for the accurate determination of Mg/Ca and Sr/Ca of marine carbonates by ICP-AES. *Geochemistry, Geophysics, Geosystems*, *3*, 623–634. https://doi.org/10.1029/2001GC000169

Dokken, T. M., & Hald, M. (1996). Rapid climatic shifts during isotope stages 2–4 in the Polar North Atlantic. *Geology*, *24*(7), 599–602. https://doi.org/10.1130/0091-7613(1996)024%3C0599:RCSDIS%3E2.3.CO;2

Dowdeswell, J. A., & Dowdeswell, E. K. (1989). Debris in icebergs and rates of glaci-marine sedimentation: Observations from Spitsbergen and a simple model. *The Journal of Geology*, *97*(2), 221–231. https://doi.org/10.1086/629296

Duplessy, J. C., Moyes, J., & Pujol, C. (1980). Deep water formation in the North Atlantic Ocean during the last ice age. *Nature*, *286*(5772), 479–482. https://doi.org/10.1038/286479a0

Eidvin, T., Jansen, E., & Riis, F. (1993). Chronology of Tertiary fan deposits off the western Barents Sea: Implications for the uplift and erosion history of the Barents Shelf. *Marine Geology*, *112*(1–4), 109–131. https://doi.org/10.1016/0025-3227(93)90164-q

Eiken, O., & Hinz, K. (1993). Contourites in the Fram Strait. *Sedimentary Geology*, *82*(1–4), 15–32. https://doi.org/10.1016/0037-0738(93)90110-q

Elliot, M., Labeyrie, L., Dokken, T., & Manthé, S. (2001). Coherent patterns of ice-rafted debris deposits in the Nordic regions during the last glacial (10–60 ka). *Earth and Planetary Science Letters*, *194*(1–2), 151–163. https://doi.org/10.1016/s0012-821x(01)00561-1

Ezat, M. M., Rasmussen, T. L., & Groeneveld, J. (2014). Persistent intermediate water warming during cold stadials in the southeastern Nordic seas during the past 65 ky. *Geology*, *42*(8), 663–666. https://doi.org/10.1130/g35579.1

Ezat, M. M., Rasmussen, T. L., & Groeneveld, J. (2016). Reconstruction of hydrographic changes in the southern Norwegian Sea during the past 135 kyr and the impact of different foraminiferal Mg/Ca cleaning protocols. *Geochemistry, Geophysics, Geosystems*, *17*(8), 3420–3436. https://doi.org/10.1002/2016gc006325

Ezat, M. M., Rasmussen, T. L., Hönisch, B., Groeneveld, J., & Demenocal, P. (2017). Episodic release of CO_2 from the high-latitude North Atlantic Ocean during the last 135 kyr. *Nature Communications*, *8*(1), 1–10. https://doi.org/10.1038/ncomms14498

Ezat, M. M., Rasmussen, T. L., Skinner, L. C., & Zamelczyk, K. (2019). Deep ocean 14C ventilation age reconstructions from the Arctic Mediterranean reassessed. *Earth and Planetary Science Letters*, *518*, 67–75. https://doi.org/10.1016/j.epsl.2019.04.027

Ezat, M. M., Rasmussen, T. L., Thornalley, D. J., Olsen, J., Skinner, L. C., Hönisch, B., & Groeneveld, J. (2017b). Ventilation history of Nordic Seas overflows during the last (de)glacial period revealed by species-specific benthic foraminiferal ^{14}C dates. *Paleoceanography*, *32*(2), 172–181. https://doi.org/10.1002/2016pa003053

Fatela, F., & Taborda, R. (2002). Confidence limits of species proportions in microfossil assemblages. *Marine Micropaleontology*, *45*(2), 169–174. https://doi.org/10.1016/s0377-8398(02)00021-x

Fossile, E., Nardelli, M. P., Jouini, A., Lansard, B., Pusceddu, A., Moccia, D., et al. (2020). Benthic foraminifera as tracers of brine production in the Storfjorden "sea ice factory". *Biogeosciences*, *17*(7), 1933–1953. https://doi.org/10.5194/bg-17-1933-2020

Ganopolski, A., & Rahmstorf, S. (2001). Rapid changes of glacial climate simulated in a coupled climate model. *Nature*, *409*(6817), 153–158. https://doi.org/10.1038/35051500

Gooday, A. J., & Hughes, J. A. (2002). Foraminifera associated with phytodetritus deposits at a bathyal site in the northern Rockall Trough (NE Atlantic): Seasonal contrasts and a comparison of stained and dead assemblages. *Marine Micropaleontology*, *46*(1–2), 83–110. https://doi.org/10.1016/s0377-8398(02)00050-6

Gooday, A. J., & Lambshead, P. J. D. (1989). Influence of seasonally deposited phytodetritus on benthic foraminiferal populations in the bathyal northeast Atlantic: The species response. *Marine Ecology Progress Series*, *58*, 53–67. https://doi.org/10.3354/meps058053

Gottschalk, J., Szidat, S., Michel, E., Mazaud, A., Salazar, G., Battaglia, M., et al. (2018). Radiocarbon measurements of small-size foraminiferal samples with the Mini Carbon Dating System (MICADAS) at the University of Bern: Implications for paleoclimate reconstructions. *Radiocarbon*, *60*(2), 469–491. https://doi.org/10.1017/rdc.2018.3

Griggs, A. J., Davies, S. M., Abbott, P. M., Rasmussen, T. L., & Palmer, A. P. (2014). Optimising the use of marine tephrochronology in the North Atlantic: A detailed investigation of the Faroe Marine Ash Zones II, III and IV. *Quaternary Science Reviews*, *106*, 122–139. https://doi.org/10.1016/j.quascirev.2014.04.031

Hald, M., & Korsun, S. (1997). Distribution of modern benthic foraminifera from fjords of Svalbard, European Arctic. *The Journal of Foraminiferal Research*, *27*(2), 101–122. https://doi.org/10.2113/gsjfr.27.2.101

Hansen, J., Ezat, M. M., Åström, E. K., & Rasmussen, T. L. (2020). New late Pleistocene species of Acharax from Arctic methane seeps off Svalbard. *Journal of Systematic Palaeontology*, *18*(2), 197–212. https://doi.org/10.1080/14772019.2019.1594420

Hasenfratz, A. P., Schiebel, R., Thornalley, D. J., Schönfeld, J., Jaccard, S. L., Martínez-García, A., et al. (2017). Mg/Ca-temperature calibration for the benthic foraminifera *Melonis barleeanum* and *Melonis pompilioides*. *Geochimica et Cosmochimica Acta*, *217*, 365–383. https://doi.org/10.1016/j.gca.2017.08.038

Heaton, T. J., Köhler, P., Butzin, M., Bard, E., Reimer, R. W., Austin, W. E., et al. (2020). Marine20 – The marine radiocarbon age calibration curve (0–55,000 cal BP). *Radiocarbon*, *62*, 1–42. https://doi.org/10.1017/rdc.2020.68

Heinrich, H. (1988). Origin and consequences of cyclic ice rafting in the northeast Atlantic Ocean during the past 130,000 years. *Quaternary Research*, *29*(2), 142–152. https://doi.org/10.1016/0033-5894(88)90057-9

Hemming, S. R. (2004). Heinrich events: Massive late Pleistocene detritus layers of the North Atlantic and their global climate imprint. *Reviews of Geophysics*, *42*, RG1005. https://doi.org/10.1029/2003rg000128

Hoff, U., Rasmussen, T. L., Stein, R., Ezat, M. M., & Fahl, K. (2016). Sea ice and millennial-scale climate variability in the Nordic seas 90 kyr ago to present. *Nature Communications*, *7*(1), 1–10. https://doi.org/10.1038/ncomms12247

Hopkins, T. S. (1991). The GIN Sea – A synthesis of its physical oceanography and literature review 1972–1985. *Earth-Science Reviews*, *30*(3–4), 175–318. https://doi.org/10.1016/0012-8252(91)90001-v

Howe, J. A., Shimmield, T. M., Harland, R. E. X., & Eyles, N. (2007). Late Quaternary contourites and glaciomarine sedimentation in the Fram Strait. *Sedimentology*, *55*(1), 179–200. https://doi.org/10.1111/j.1365-3091.2007.00897.x

Huber, C., Leuenberger, M., Spahni, R., Flückiger, J., Schwander, J., Stocker, T. F., et al. (2006). Isotope calibrated Greenland temperature record over Marine Isotope Stage 3 and its relation to CH_4. *Earth and Planetary Science Letters*, *243*(3–4), 504–519. https://doi.org/10.1016/j.epsl.2006.01.002

Hughes, A. L., Gyllencreutz, R., Lohne, Ø. S., Mangerud, J., & Svendsen, J. I. (2016). The last Eurasian ice sheets – A chronological database and time-slice reconstruction, DATED-1. *Boreas*, *45*(1), 1–45. https://doi.org/10.1111/bor.12142

Jansen, E., Sejrup, H.-P., Fjæran, T., Hald, M., Holtedahl, H., & Skarbø, O. (1983). Late Weichselian paleoceanography of the southeastern Norwegian Sea. *Norsk Geologisl Tidsskrift*, *63*, 117–146.

Jennings, A. E., & Helgadottir, G. (1994). Foraminiferal assemblages from the fjords and shelf of eastern Greenland. *The Journal of Foraminiferal Research*, *24*(2), 123–144. https://doi.org/10.2113/gsjfr.24.2.123

Jennings, A. E., Weiner, N. J., Helgadottir, G., & Andrews, J. T. (2004). Modern foraminiferal faunas of the southwestern to northern Iceland shelf: Oceanographic and environmental controls. *The Journal of Foraminiferal Research*, *34*(3), 180–207. https://doi.org/10.2113/34.3.180

Jensen, M. F., Nilsson, J., & Nisancioglu, K. H. (2016). The interaction between sea ice and salinity-dominated ocean circulation: Implications for halocline stability and rapid changes of sea ice cover. *Climate Dynamics*, *47*(9–10), 3301–3317. https://doi.org/10.1007/s00382-016-3027-5

Jernas, P., Klitgaard-Kristensen, D., Husum, K., Koç, N., Tverberg, V., Loubere, P., et al. (2018). Annual changes in Arctic fjord environment and modern benthic foraminiferal fauna: Evidence from Kongsfjorden, Svalbard. *Global and Planetary Change*, *163*, 119–140. https://doi.org/10.1016/j.gloplacha.2017.11.013

Jessen, S. P., & Rasmussen, T. L. (2019). Ice-rafting patterns on the western Svalbard slope 74–0 ka: Interplay between ice-sheet activity, climate and ocean circulation. *Boreas*, *48*(1), 236–256. https://doi.org/10.1111/bor.12358

Jessen, S. P., Rasmussen, T. L., Nielsen, T., & Solheim, A. (2010). A new Late Weichselian and Holocene marine chronology for the western Svalbard slope 30,000–0 cal years BP. *Quaternary Science Reviews*, *29*(9–10), 1301–1312. https://doi.org/10.1016/j.quascirev.2010.02.020

Johnsen, S. J., Clausen, H. B., Dansgaard, W., Fuhrer, K., Gundestrup, N., Hammer, C. U., et al. (1992). Irregular glacial interstadials recorded in a new Greenland ice core. *Nature*, *359*(6393), 311–313. https://doi.org/10.1038/359311a0

Johnsen, S. J., Dahl-Jensen, D., Gundestrup, N., Steffensen, J. P., Clausen, H. B., Miller, H., et al. (2001). Oxygen isotope and palaeotemperature records from six Greenland ice-core stations: Camp Century, Dye-3, GRIP, GISP2, Renland and NorthGRIP. *Journal of Quaternary Science*, *16*(4), 299–307. https://doi.org/10.1002/jqs.622

Kindler, P., Guillevic, M., Baumgartner, M. F., Schwander, J., Landais, A., & Leuenberger, M. (2014). Temperature reconstruction from 10 to 120 kyr b2k from the NGRIP ice core. *Climate of the Past*, *10*(2), 887–902. https://doi.org/10.5194/cp-10-887-2014

Knies, J., Köseoğlu, D., Rise, L., Baeten, N., Bellec, V. K., Bøe, R., et al. (2018). Nordic Seas polynyas and their role in preconditioning marine productivity during the Last Glacial Maximum. *Nature Communications*, *9*(1), 1–10. https://doi.org/10.1038/s41467-018-06252-8

Knutti, R., Flückiger, J., Stocker, T. F., & Timmermann, A. (2004). Strong hemispheric coupling of glacial climate through freshwater discharge and ocean circulation. *Nature*, *430*(7002), 851–856. https://doi.org/10.1038/nature02786

Korsun, S., & Hald, M. (1998). Modern benthic foraminifera off Novaya Zemlya tidewater glaciers, Russian Arctic. *Arctic and Alpine Research*, *30*(1), 61–77. https://doi.org/10.2307/1551746

Korsun, S., & Hald, M. (2000). Seasonal dynamics of benthic foraminifera in a glacially fed fjord of Svalbard, European Arctic. *The Journal of Foraminiferal Research*, *30*(4), 251–271. https://doi.org/10.2113/0300251

Kristjánsdóttir, G. B., Lea, D. W., Jennings, A. E., Pak, D. K., & Belanger, C. (2007). New spatial Mg/Ca-temperature calibrations for three Arctic, benthic foraminifera and reconstruction of north Iceland shelf temperature for the past 4000 years. *Geochemistry, Geophysics, Geosystems*, *8*, Q03P21. https://doi.org/10.1029/2006gc001425

Laberg, J. S., & Vorren, T. O. (1995). Late Weichselian submarine debris flow deposits on the Bear Island Trough mouth fan. *Marine Geology*, *127*(1–4), 45–72. https://doi.org/10.1016/0025-3227(95)00055-4

Landais, A., Masson-Delmotte, V., Jouzel, J., Raynaud, D., Johnsen, S., Huber, C., et al. (2006). The glacial inception as recorded in the NorthGRIP Greenland ice core: Timing, structure and associated abrupt temperature changes. *Climate Dynamics*, *26*(2–3), 273–284. https://doi.org/10.1007/s00382-005-0063-y

Lekens, W. A., Sejrup, H. P., Haflidason, H., Knies, J., & Richter, T. (2006). Meltwater and ice rafting in the southern Norwegian Sea between 20 and 40 calendar kyr B.P.: Implications for Fennoscandian Heinrich events. *Paleoceanography*, *21*, PA3013. https://doi.org/10.1029/2005pa001228

Li, C., & Born, A. (2019). Coupled atmosphere-ice-ocean dynamics in Dansgaard-Oeschger events. *Quaternary Science Reviews*, *203*, 1–20. https://doi.org/10.1016/j.quascirev.2018.10.031

Linke, P., & Lutze, G. F. (1993). Microhabitat preferences of benthic foraminifera – A static concept or a dynamic adaptation to optimize food acquisition? *Marine Micropaleontology*, *20*(3–4), 215–234. https://doi.org/10.1016/0377-8398(93)90034-u

Locarnini, R. A., Mishonov, A. V., Baranova, O. K., Boyer, T. P., Zweng, M. M., Garcia, H. E., et al. (2018). World Ocean Atlas 2018. In A. Mishonov Technical (Ed.), *NOAA Atlas NESDIS 81*(Volume 1: Temperature, p. 52).

Lubinski, D. J., Polyak, L., & Forman, S. L. (2001). Freshwater and Atlantic water inflows to the deep northern Barents and Kara seas since ca 13 ^{14}C ka: Foraminifera and stable isotopes. *Quaternary Science Reviews*, *20*(18), 1851–1879. https://doi.org/10.1016/s0277-3791(01)00016-6

Mackensen, A., & Hald, M. (1988). *Cassidulina teretis* Tappan and *C. laevigata* d'Orbigny; their modern and late Quaternary distribution in northern seas. *The Journal of Foraminiferal Research*, *18*(1), 16–24. https://doi.org/10.2113/gsjfr.18.1.16

Mackensen, A., & Schmiedl, G. (2016). Brine formation recorded by stable isotopes of recent benthic foraminifera in Storfjorden, Svalbard: Palaeoceanographical implications. *Boreas*, *45*(3), 552–566. https://doi.org/10.1111/bor.12174

Mackensen, A., & Schmiedl, G. (2019). Stable carbon isotopes in paleoceanography: Atmosphere, oceans, and sediments. *Earth-Science Reviews*, *197*, 102893. https://doi.org/10.1016/j.earscirev.2019.102893

Mackensen, A., Schumacher, S., Radke, J., & Schmidt, D. N. (2000). Microhabitat preferences and stable carbon isotopes of endobenthic foraminifera: Clue to quantitative reconstruction of oceanic new production? *Marine Micropaleontology*, *40*(3), 233–258. https://doi.org/10.1016/s0377-8398(00)00040-2

Mackensen, A., Sejrup, H. P., & Jansen, E. (1985). The distribution of living benthic foraminifera on the continental slope and rise off southwest Norway. *Marine Micropaleontology*, *9*(4), 275–306. https://doi.org/10.1016/0377-8398(85)90001-5

Marcott, S. A., Clark, P. U., Padman, L., Klinkhammer, G. P., Springer, S. R., Liu, Z., et al. (2011). Ice-shelf collapse from subsurface warming as a trigger for Heinrich events. *Proceedings of the National Academy of Sciences of the United States of America*, *108*(33), 13415–13419. https://doi.org/10.1073/pnas.1104772108

McCorkle, D. C., Keigwin, L. D., Corliss, B. H., & Emerson, S. R. (1990). The influence of microhabitats on the carbon isotopic composition of deep-sea benthic foraminifera. *Paleoceanography*, *5*(2), 161–185. https://doi.org/10.1029/pa005i002p00161

Mudie, P. J., Keen, C. E., Hardy, I. A., & Vilks, G. (1984). Multivariate analysis and quantitative paleoecology of benthic foraminifera in surface and Late Quaternary shelf sediments, northern Canada. *Marine Micropaleontology*, *8*(4), 283–313. https://doi.org/10.1016/0377-8398(84)90018-5

Müller, J., & Stein, R. (2014). High-resolution record of late glacial and deglacial sea ice changes in Fram Strait corroborates ice-ocean interactions during abrupt climate shifts. *Earth and Planetary Science Letters*, *403*, 446–455. https://doi.org/10.1016/j.epsl.2014.07.016

Ottesen, D., Dowdeswell, J. A., & Rise, L. (2005). Submarine landforms and the reconstruction of fast-flowing ice streams within a large Quaternary ice sheet: The 2500-km-long Norwegian-Svalbard margin (57°–80°N). *Geological Society of America Bulletin*, *117*(7–8), 1033–1050. https://doi.org/10.1130/b25577.1

Pena, L. D., Calvo, E., Cacho, I., Eggins, S., & Pelejero, C. (2005). Identification and removal of Mn-Mg-rich contaminant phases on foraminiferal tests: Implications for Mg/Ca past temperature reconstructions. *Geochemistry, Geophysics, Geosystems*, *6*, Q09P02. https://doi.org/10.1029/2005gc000930

Polyak, L., Best, K. M., Crawford, K. A., Council, E. A., & St-Onge, G. (2013). Quaternary history of sea ice in the western Arctic Ocean based on foraminifera. *Quaternary Science Reviews*, *79*, 145–156. https://doi.org/10.1016/j.quascirev.2012.12.018

Polyak, L., Korsun, S., Febo, L. A., Stanovoy, V., Khusid, T., Hald, M., et al. (2002). Benthic foraminiferal assemblages from the southern Kara Sea, a river-influenced Arctic marine environment. *The Journal of Foraminiferal Research*, *32*(3), 252–273. https://doi.org/10.2113/32.3.252

Polyak, L., & Mikhailov, V. (1996). Post-glacial environments of the southeastern Barents Sea: Foraminiferal evidence. *Geological Society, London, Special Publications*, *111*(1), 323–337. https://doi.org/10.1144/gsl.sp.1996.111.01.21

Rasmussen, S. O., Bigler, M., Blockley, S. P., Blunier, T., Buchardt, S. L., Clausen, H. B., et al. (2014a). A stratigraphic framework for abrupt climatic changes during the Last Glacial period based on three synchronized Greenland ice-core records: Refining and extending the INTIMATE event stratigraphy. *Quaternary Science Reviews*, *106*, 14–28. https://doi.org/10.1016/j.quascirev.2014.09.007

Rasmussen, T. L., Oppo, D. W., Thomsen, E., & Lehman, S. J. (2003). Deep sea records from the southeast Labrador Sea: Ocean circulation changes and ice-rafting events during the last 160,000 years. *Paleoceanography*, *18*, 10181. https://doi.org/10.1029/2001pa000736

Rasmussen, T. L., & Thomsen, E. (2004). The role of the North Atlantic Drift in the millennial timescale glacial climate fluctuations. *Palaeogeography, Palaeoclimatology, Palaeoecology*, *210*(1), 101–116. https://doi.org/10.1016/j.palaeo.2004.04.005

Rasmussen, T. L., & Thomsen, E. (2009). Stable isotope signals from brines in the Barents Sea: Implications for brine formation during the last glaciation. *Geology*, *37*(10), 903–906. https://doi.org/10.1130/g25543a.1

Rasmussen, T. L., & Thomsen, E. (2013). Pink marine sediments reveal rapid ice melt and Arctic meltwater discharge during Dansgaard–Oeschger warmings. *Nature Communications*, *4*(1), 1–8. https://doi.org/10.1038/ncomms3849

Rasmussen, T. L., & Thomsen, E. (2017). Ecology of deep-sea benthic foraminifera in the North Atlantic during the last glaciation: Food or temperature control. *Palaeogeography, Palaeoclimatology, Palaeoecology*, *472*, 15–32. https://doi.org/10.1016/j.palaeo.2017.02.012

Rasmussen, T. L., Thomsen, E., Labeyrie, L., & van Weering, T. C. (1996a). Circulation changes in the Faeroe-Shetland Channel correlating with cold events during the last glacial period (58–10 ka). *Geology*, *24*(10), 937–940. https://doi.org/10.1130/0091-7613(1996)024%3C0937:ccitfs%3E2.3.co;2

Rasmussen, T. L., Thomsen, E., van Weering, T. C., & Labeyrie, L. (1996b). Rapid changes in surface and deep water conditions at the Faeroe Margin during the last 58,000 years. *Paleoceanography*, *11*(6), 757–771. https://doi.org/10.1029/96pa02618

Rasmussen, T. L., Thomsen, E., & Nielsen, T. (2014b). Water mass exchange between the Nordic seas and the Arctic Ocean on millennial timescale during MIS 4–MIS 2. *Geochemistry, Geophysics, Geosystems*, *15*(3), 530–544. https://doi.org/10.1002/2013gc005020

Rasmussen, T. L., Thomsen, E., Ślubowska, M. A., Jessen, S., Solheim, A., & Koç, N. (2007). Paleoceanographic evolution of the SW Svalbard margin (76°N) since 20,000 ^{14}C yr BP. *Quaternary Research*, *67*(1), 100–114. https://doi.org/10.1016/j.yqres.2006.07.002

Rudels, B. (1987). On the mass balance of the Polar Ocean, with special emphasis on the Fram Strait. *Norsk Polarinstitutt Skrifter, No. 188*. Retrieved from http://hdl.handle.net/11250/173528

Rudels, B., Jones, E. P., Schauer, U., & Eriksson, P. (2004). Atlantic sources of the Arctic Ocean surface and halocline waters. *Polar Research*, *23*(2), 181–208. https://doi.org/10.3402/polar.v23i2.6278

Ruff, M., Szidat, S., Gäggeler, H. W., Suter, M., Synal, H. A., & Wacker, L. (2010). Gaseous radiocarbon measurements of small samples. *Nuclear Instruments and Methods in Physics Research Section B: Beam Interactions with Materials and Atoms*, *268*(7–8), 790–794. https://doi.org/10.1016/j.nimb.2009.10.032

Sadatzki, H., Dokken, T. M., Berben, S. M., Muschitiello, F., Stein, R., Fahl, K., et al. (2019). Sea ice variability in the southern Norwegian Sea during glacial Dansgaard-Oeschger climate cycles. *Science Advances*, *5*(3), eaau6174. https://doi.org/10.1126/sciadv.aau6174

Sarnthein, M., Stattegger, K., Dreger, D., Erlenkeuser, H., Grootes, P., Haupt, B. J., et al. (2001). Fundamental modes and abrupt changes in North Atlantic circulation and climate over the last 60 ky – Concepts, reconstruction and numerical modeling. In P. Schäfer W. Ritzrau M. Schlüter & J. Thiede (Eds.), *The Northern North Atlantic* (pp. 365–410). Berlin, Heidelberg: Springer. https://doi.org/10.1007/978-3-642-56876-3_21

Schönfeld, J. (2001). Benthic foraminifera and pore-water oxygen profiles: A re-assessment of species boundary conditions at the western Iberian margin. *The Journal of Foraminiferal Research*, *31*(2), 86–107. https://doi.org/10.2113/0310086

Seidenkrantz, M. S. (1995). *Cassidulina teretis* Tappan and *Cassidulina neoteretis* new species (Foraminifera): Stratigraphic markers for deep sea and outer shelf areas. *Journal of Micropalaeontology*, *14*(2), 145–157. https://doi.org/10.1144/jm.14.2.145

Seidenkrantz, M. S. (2013). Benthic foraminifera as palaeo sea-ice indicators in the subarctic realm-examples from the Labrador Sea-Baffin Bay region. *Quaternary Science Reviews*, *79*, 135–144. https://doi.org/10.1016/j.quascirev.2013.03.014

Sejrup, H. P., Fjaeran, T., Hald, M., Beck, L., Hagen, J., Miljeteig, I., et al. (1981). Benthonic foraminifera in surface samples from the Norwegian continental margin between 62 degrees N and 65 degrees N. *The Journal of Foraminiferal Research*, *11*(4), 277–295. https://doi.org/10.2113/gsjfr.11.4.277

Sessford, E. G., Jensen, M. F., Tisserand, A. A., Muschitiello, F., Dokken, T., Nisancioglu, K. H., & Jansen, E. (2019). Consistent fluctuations in intermediate water temperature off the coast of Greenland and Norway during Dansgaard-Oeschger events. *Quaternary Science Reviews*, *223*, 105887. https://doi.org/10.1016/j.quascirev.2019.105887

Sessford, E. G., Tisserand, A. A., Risebrobakken, B., Andersson, C., Dokken, T., & Jansen, E. (2018). High-resolution Benthic Mg/Ca temperature record of the intermediate water in the Denmark Strait Across D-O stadial-interstadial cycles. *Paleoceanography and Paleoclimatology*, *33*(11), 1169–1185. https://doi.org/10.1029/2018pa003370

Sherriff-Tadano, S., Abe-Ouchi, A., & Oka, A. (2020). Impact of mid-glacial ice sheets on deep ocean circulation and global climate: Role of surface cooling on the AMOC. *Climate of the Past Discussions*, *17*, 1–28. https://doi.org/10.5194/cp-2020-75

Stanford, J. D., Rohling, E. J., Bacon, S., Roberts, A. P., Grousset, F. E., & Bolshaw, M. (2011). A new concept for the paleoceanographic evolution of Heinrich event 1 in the North Atlantic. *Quaternary Science Reviews*, *30*(9–10), 1047–1066. https://doi.org/10.1016/j.quascirev.2011.02.003

Steinsund, P. I. (1994). *Benthic foraminifera in surface sediments of the Barents and Kara seas: Modern and late Quaternary applications* (Unpublished PhD thesis). Norway: University of Tromsø.

Svensson, A., Andersen, K. K., Bigler, M., Clausen, H. B., Dahl-Jensen, D., Davies, S. M., et al. (2008). A 60 000 year Greenland stratigraphic ice core chronology. *Climate of the Past*, *4*(1), 47–57. https://doi.org/10.5194/cp-4-47-2008

Sztybor, K., & Rasmussen, T. L. (2017). Late glacial and deglacial palaeoceanographic changes at Vestnesa Ridge, Fram Strait: Methane seep versus non-seep environments. *Palaeogeography, Palaeoclimatology, Palaeoecology*, *476*, 77–89. https://doi.org/10.1016/j.palaeo.2017.04.001

Thomsen, E., Rasmussen, T. L., Sztybor, K., Hanken, N. M., Tendal, O. S., & Uchman, A. (2019). Cold-seep fossil macrofaunal assemblages from Vestnesa Ridge, eastern Fram Strait, during the past 45 000 years. *Polar Research*, *38*, 3310. https://doi.org/10.33265/polar.v38.3310

Thornalley, D. J., Bauch, H. A., Gebbie, G., Guo, W., Ziegler, M., Bernasconi, S. M., et al. (2015). A warm and poorly ventilated deep Arctic Mediterranean during the last glacial period. *Science*, *349*(6249), 706–710. https://doi.org/10.1126/science.aaa9554

Vogt, P. R., Crane, K., Sundvor, E., Max, M. D., & Pfirman, S. L. (1994). Methane-generated (?) pockmarks on young, thickly sedimented oceanic crust in the Arctic: Vestnesa ridge, Fram strait. *Geology*, *22*(3), 255–258. https://doi.org/10.1130/0091-7613(1994)022%3C0255:mgpoyt%3E2.3.co;2

Vorren, T. O., Laberg, J. S., Blaume, F., Dowdeswell, J. A., Kenyon, N. H., Mienert, J., et al. (1998). The Norwegian–Greenland Sea continental margins: Morphology and late Quaternary sedimentary processes and environment. *Quaternary Science Reviews*, *17*(1–3), 273–302. https://doi.org/10.1016/s0277-3791(97)00072-3

Wary, M., Eynaud, F., Rossignol, L., Zaragosi, S., Sabine, M., Castera, M. H., & Billy, I. (2017). The southern Norwegian Sea during the last 45 ka: Hydrographical reorganizations under changing ice-sheet dynamics. *Journal of Quaternary Science*, *32*(7), 908–922. https://doi.org/10.1002/jqs.2965

Wastegård, S., & Rasmussen, T. L. (2014). Faroe Marine Ash Zone IV: A new MIS 3 ash zone on the Faroe Islands margin. *Geological Society, London, Special Publications*, *398*(1), 81–93. https://doi.org/10.1144/sp398.3

Wefer, G., Heinze, P. M., & Berger, W. H. (1994). Clues to ancient methane release. *Nature*, *369*(6478), 282. https://doi.org/10.1038/369282a0

Winsborrow, M. C., Andreassen, K., Corner, G. D., & Laberg, J. S. (2010). Deglaciation of a marine-based ice sheet: Late Weichselian palaeo-ice dynamics and retreat in the southern Barents Sea reconstructed from onshore and offshore glacial geomorphology. *Quaternary Science Reviews*, *29*(3–4), 424–442. https://doi.org/10.1016/j.quascirev.2009.10.001

Wolff, E. W., Chappellaz, J., Blunier, T., Rasmussen, S. O., & Svensson, A. (2010). Millennial-scale variability during the last glacial: The ice core record. *Quaternary Science Reviews*, *29*(21–22), 2828–2838. https://doi.org/10.1016/j.quascirev.2009.10.013

Wollenburg, J. E., Knies, J., & Mackensen, A. (2004). High-resolution paleoproductivity fluctuations during the past 24 kyr as indicated by benthic foraminifera in the marginal Arctic Ocean. *Palaeogeography, Palaeoclimatology, Palaeoecology*, *204*(3–4), 209–238. https://doi.org/10.1016/s0031-0182(03)00726-0

Wollenburg, J. E., & Kuhnt, W. (2000). The response of benthic foraminifers to carbon flux and primary production in the Arctic Ocean. *Marine Micropaleontology*, *40*(3), 189–231. https://doi.org/10.1016/s0377-8398(00)00039-6

Wollenburg, J. E., Kuhnt, W., & Mackensen, A. (2001). Changes in Arctic Ocean paleoproductivity and hydrography during the last 145 kyr: The benthic foraminiferal record. *Paleoceanography*, *16*(1), 65–77. https://doi.org/10.1029/1999pa000454

Wollenburg, J. E., & Mackensen, A. (1998). Living benthic foraminifers from the central Arctic Ocean: Faunal composition, standing stock and diversity. *Marine Micropaleontology*, *34*(3–4), 153–185. https://doi.org/10.1016/s0377-8398(98)00007-3

References From the Supporting Information

GEOSECS Executive Committee. (1987). GEOSECS Atlantic, Pacific, and Indian Ocean Expeditions, vol. 7, Shorebased Data and Graphics, p. 100. Washington, DC: National Science Foundation.

O'Neil, J. R., Clayton, R. N., & Mayeda, T. K. (1969). Oxygen isotope fractionation in divalent metal carbonates. *The Journal of Chemical Physics*, *51*(12), 5547–5558. https://doi.org/10.1063/1.1671982

Shackleton, N. J. (1974). Attainment of isotopic equilibrium between ocean water and the benthonic foraminifera genus *Uvigerina*: Isotopic changes in the ocean during the last glacial. *Colloques Internationaux du CNRS*. (219).

Spratt, R. M., & Lisiecki, L. E. (2016). A Late Pleistocene sea level stack. *Climate of the Past*, *12*(4), 1079–1092. https://doi.org/10.5194/cpd-11-3699-2015